A NUMERICAL MODELING ANALYSIS OF THE SAN FRANCISCO BAY AND SACRAMENTO-SAN JOAQUIN DELTA: RIVERINE, TIDAL, AND WIND PROCESSES

A Thesis

presented to

the Faculty of California Polytechnic State University,

San Luis Obispo

In Partial Fulfillment

of the Requirements for the Degree

Master of Science in Civil and Environmental Engineering

by

Drake Abrahamsson

December 2023

COMMITTEE MEMBERSHIP

TITLE:	A Numerical Modeling Analysis of the San Francisco Bay and Sacramento-San Joaquin Delta: Riverine, Tidal, and Wind Processes
AUTHOR:	Drake Abrahamsson
DATE SUBMITTED:	December 2023
COMMITTEE CHAIR:	Stefan Talke, Ph.D Professor of Civil Engineering
COMMITTEE MEMBER:	Misgana Muleta, Ph.D Professor and Chair of Civil Engineering
COMMITTEE MEMBER:	Ryan Walter, Ph.D Associate Professor of Physics

ABSTRACT

A Numerical Model Analysis of the San Francisco Bay and Sacramento-San Joaquin Delta

Drake Abrahamsson

The primary motivation of this study is to analyze the 1D-2DH hydrodynamic model of the San Francisco Bay and Sacramento-San Joaquin Delta (SFBD) outlined in Nederhoff et al. (2021). I compared model water level data to 70 tidal records from the National Oceanic and Atmospheric Association (NOAA), the United States Geological Survey (USGS), the California Data Exchange Center (CDEC), and from local municipalities throughout the Bay Area to investigate how the model captures water levels and tidal constituent amplitudes. While the Nederhoff et al (2017) model analyzed an extended time period from 1950-2019, I analyzed M2 amplitude and tidal water levels for the water year of 2017 (WY2017) with a larger dataset that extended into the Sacramento-San Joaquin Delta. Because WY2017 was a high river flow year for the Sacramento Delta, the model was able to be evaluated throughout a large range of flow regimes.

I used harmonic analysis through the MATLAB package UTide (Codiga et al. 2011) to assess the model's ability to replicate M2 amplitudes. I assessed the error for these M2 values as well as for tidal water levels. The average RMSE for M2 amplitude is 0.111 m across the entire model domain during WY2017, performing fairly consistent throughout the model. The one exception being the shallow and complex Grizzly Bay, which performed significantly worse, with RMSE values around 0.5 m. The model better replicated water levels in the 2DH grid representation of the San Francisco Bay (<0.1 m RMSE), while the 1D representation of the Sacramento-San Joaquin Delta saw RMSE values typically around 0.15 m. Qualitatively, the model captured the inverse relationship between river flow and the M2 amplitude throughout the entire year at a vast majority of the 70 observed stations. Therefore, it is appropriate for investigating how riverine, oceanic, and atmospheric processes influence high water levels throughout the SFBD.

Attempts to improve the model were mostly unsuccessful. I tried to increase the grid resolution at the Carquinez Strait to improve tidal propagation upstream, but altering the grid caused the coupling between the 2DH grid and 1D network to detach. This prevented the propagation of water flow in either direction at the coupling near Collinsville. The software required to fix this coupling was non-standard and unavailable for my usage, so I was unable to resolve the issue. I also attempted to create a new wind forcing file using in-situ data rather than the ERA5 reanalysis. This new wind forcing made negligible difference in water level and M2 model skill.

An experiment in removing river flow showed that riverine impacts on elevating extreme water levels only have effects (>0.05 m) east of the Carquinez Strait. Extreme water levels west of this point in the San Pablo, Central, and South Bays are dominated by tides, storm surge, and to a lesser extent local wind. A decrease in tidal amplitude by river flow potentially decreases flood risk in some parts of the Bay during times of high outflow from the Sacramento-San Joaquin Delta. I also investigated maximum equilibrium effects of constant wind in the two prevailing wind directions (southerly and westerly) of the San Francisco Bay. The wind setup effect become more prominent (>0.05 m) at and above a steady 10 m/s in both directions. This study also showed that wind likely exerts a small influence on tidal properties, especially for winds greater than 10 m/s.

Keywords: San Francisco Bay, Sacramento-San Joaquin Delta, Tidal Analysis, Extreme Water Levels, Hydrodynamic Modeling

ACKNOWLEDGMENTS

I would like to thank my committee chair, Dr. Stefan Talke, for his knowledge and expertise that guided me through the exploration of this research. I would also like to thank Dr. Serena Lee for her generosity of time spent helping me improve my coding skills. Both pushed me throughout my graduate degree to refine my knowledge and the final product of this thesis. This truly would not have been possible without these wonderful mentors.

I would also like to thank my other committee members, Dr. Misgana Muleta and Dr. Ryan Walter, for their scheduling flexibility and support throughout the last year. Their accomplished backgrounds and perspectives were invaluable to my research.

And finally, to my family and girlfriend: your unending love, support, and understanding have made all the difference in this journey. Thank you for always putting a smile on my face and a spark in my step, even during the most challenging parts of my graduate education. I am looking forward to being able to spend more time with you now!

TABLE OF CONTENTS

LIST OF TABLES

LIST OF FIGURES

Chapter 1

INTRODUCTION

1.1 Background

Estuaries are systems where freshwater meet oceanic seawater [1]. The San Francisco Bay is the largest estuary on the west coast of North America and is located in Northern California. Tides from the Pacific Ocean enter the San Francisco Bay at the Golden Gate Strait. Freshwater delta river flow enters the bay from the Sacramento and San Joaquin Rivers. Smaller tributaries such as Coyote Creek and the Mokelumne River drain into various locations throughout the San Francisco Bay.

Water levels in estuaries are influenced by tidal, riverine, and atmospheric processes. Tidal processes drive water level at a sub-daily scale. At the Golden Gate Strait, the tidal range is roughly 2 meters. Due to tidal wave reflection, the tidal range at the far south end of the South San Francisco Bay (SSFB) exceeds the tidal range at the Golden Gate Strait by nearly 0.6 m [2]. As tidal waves travel upstream, they are dampened by adverse effects such as friction and river flow. The tidal signal appears as far into the Sacramento-San Joaquin Delta as 180km upstream from the Golden Gate Bridge (GGB) [3]. However, the strength and extent of the tidal signal throughout the estuary is responsive to the river flow in the system [4].

The riverine forcing that influences water levels is mainly driven by the Sacramento-San Joaquin Delta, but small creek flow from the surrounding Bay Area is also influential. The outflow from the Sacramento-San Joaquin Delta to the San Francisco Bay is monitored and defined as Net Delta Outflow (NDO) [5]. For the 2017 water year (WY2017), the NDO had an average flowrate of 1,902 cubic meters per second (m^3/s). For scale, for WY2017, the smaller tributaries had average flows on the scale of 0.05-15 m^3/s. Delta river flow is the main mechanism for flooding within the Sacramento-San Joaquin Delta component of the estuary. The closer to the ocean that is analyzed, the less impact river flow has on extreme water levels. Tidal and atmospheric forcings begin to dominate instead.

Atmospheric processes such as wind affect water levels in estuaries such as the San Francisco Bay [6], [7]. Temporary water level changes can be caused by wind in basins and estuaries. Wind stress is exerted on the surface of the water, eventually accumulating at the leeward side of the basin, and dispersing from the windward side, creating a slope across the basin. This effect is known as wind setup. Once the wind subsides, the water levels are pulled back to equilibrium by gravity but overshoot due to inertia. This causes a standing wave known as a seiche, that dissipates until the water reaches equilibrium [8]. The primary direction of wind (westerly) in the San Francisco Bay aligns with the Northern Reach of the SF Bay, but during storm events, a southerly wind can align with the long fetch of the South, Central, and San Pablo Bays. The long fetch of this N-S orientation leaves room for large wind setup potential given optimal wind direction, and magnitude.

1.2 Research Questions

The following research questions were investigated using a combination of data analysis and simulation experiments using the Nederhoff et al. (2021) hydrodynamic numerical model. How does the tidal range and mean water level respond to increased river flow? The WY 2017, a high river flow year for the San Francisco Bay, was analyzed to evaluate the nonlinear interactions of river flow and tidal forcing in the Bay Area. Utilizing short term harmonic analysis (~32-day analysis periods with 1-day timesteps), I assessed the response of the M2 amplitude and mean water levels to the widely variable flow regimes of WY 2017. I assessed the M2 amplitude because it is the largest constituent in San Francisco Bay and because of its known sensitivity to river flow [4]. Where do tides and river flow effects dominate extreme water levels throughout the San Francisco Bay Area (SFBD)? Tidal and riverine forcings were isolated by removing or altering flowrates from the Sacramento-San Joaquin Delta for WY2017 simulations. This isolation allowed for the examination of the differences in extreme water levels between the complete and altered simulations. To what degree does wind affect extreme water levels and does the model replicate these effects? Experiments with constant wind were simulated to analyze the effects of westerly and southerly winds on extreme water levels. Can the hydrodynamic numerical model outlined in Nederhoff et al. (2021) be improved? The model is

detailed further in sections 2.3.7,3.1, and 3.2. Based on the initial performance of the model, I attempted to make improvements to the grid in areas that were not conveying enough water upstream. The ERA5 wind forcing used in the model showed large discrepancies for both direction and magnitude. I created a new wind forcing file with data directly from several wind gauges throughout the model domain. In an attempt to increase tidal propagation upstream, I attempted to improve the grid by doubling the grid resolution across the narrowest point of the Bay Area, the Carquinez Strait.

Chapter 2

LITERATURE REVIEW

2.1 Theory Review

Information on other estuaries or general knowledge of important estuarine processes can give insight into the hydrodynamics of the SFBD. This section will cover existing knowledge and science that provides insights into the unique functioning of the SFBD.

2.1.1 Estuaries

Estuaries are partially enclosed coastal areas where riverine freshwater converges with oceanic salt water [9]. For a coastal plain estuary or drowned, tectonically reshaped river valley such as San Francisco Bay [10], water motion is primarily driven by oceanic tides and upstream freshwater discharge [11]. Depending on the location within the estuary, one of these forcing factors will usually control currents and water levels. Tides lose energy as they propagate upstream due to bottom friction and nonlinear interaction with river flow [12], [13]. However, tidal amplitudes may reduce, stay the same, or even amplify, depending on factors such as the convergence rate of bathymetry and reflection/resonance effects [14]–[17]. Currents and frictional forces are greatly increased in areas with decreased cross-sectional area, such as the narrow and shallow Carquinez Strait in the San Francisco Bay.

2.1.2 Tides in Estuaries

Tides, determined by astronomical forcings, are one of the major forcings that determine water levels in estuaries [15]. The gravitational forcing of the moon, earth, and suns' orbits produces tides. These tides interact with oceanic bathymetry and continental margins to produce tidal motions. These tidal motions are represented by hundreds of sinusoids. These sinusoids are called constituents and can be summed to represent the complete tidal cycle. The primary dominant tidal constituents are M2, S2, K1, N2, M4, and M2. The M2 tide is the largest constituent along the U.S. West coast, followed by K1 [18]. The M2 is sensitive to river flow and can be used as an indicator of how well a model is recreating observed tidal conditions [4], [8].

The number in each tidal constituent indicates approximately how many times they repeat in a 24 hour, 50-minute (~1 day) cycle. For example, M2, the principle semidiurnal lunar tidal constituent, repeats about twice a day. K1, the principle lunar diurnal tidal constituent, repeats about once a day (diurnal == daily). Other constituents such as S2 account for solar gravity effects. Particularly in shallow waters (e.g., estuaries), nonlinear effects such as friction commonly produce constituents which are combinations of other constituents. Such shallow water constituents include overtides, which are higher harmonics of the main tidal constituents [8]. They are formed when a single constituent frequency interacts with non-linear forcings [19]. For example, the tidal constituent M4 is an overtide of M2, with a period that is ½ that of M2. Offset phases of overtides contribute to tidal asymmetry. On the U.S. West Coast, the phasing of the lunar and lunisolar diurnal tides (K1 and O1, respectively) and M2 also produce tidal wave asymmetry [18]. This tidal asymmetry is one of the most important processes in creating sediment transport in estuaries [20], [21].

When tides interact with shallow water and other geographic features present in estuaries, more complicated interactions and changes to tidal motions occur. Once the tidal wave enters the riverine portion of an estuary, the effect of astronomical forcing is negligible, and the tide will eventually diminish as it travels further upstream, in the absence of a reflective barrier [13]. The tidal range (tidal wave amplitude) in estuaries is affected by five dominant, interacting processes [12], [14], [16], [22], [23]:

- Inertial effects (e.g., advective acceleration)
- Converging and diverging channel width and depth
- Bottom friction
- Reflection at the landward boundary
- River flow

Inertial effects refer to the mass*acceleration portion of the equation of motion and refer to the tendency of an object (such as a parcel of water) to stay in motion if not acted on by an external force. Factors that produce a change in velocity (an acceleration), such as a change in

geometry, must be balanced by a force. Increasing river discharge increases tidal dampening through nonlinear convective inertia and bottom friction. Additionally, momentum is lost as water moves over tidal flats because of strong friction [12]. Estuaries with deeper channels will conserve inertia further upstream, maintaining a larger tidal range. In a straight waterway where the depth is much greater than the amplitude of the tidal wave, the inertial terms can be neglected [22]. However, exclusion of the convective inertial term has been shown to yield an underestimation of tidal dampening [24].

Converging and diverging shorelines can affect the tides in multiple ways, producing either amplification or attenuation [16]. In a frictionless system, the tidal amplitude increases for decreasing width and depth [12]. However, the frictional forces usually dominate in a real-world system. Whether depth and width convergence increases or decreases the tidal amplitude is dependent on the magnitude of friction [12], [16]. Equation 1 determines whether the tidal amplitude is amplified or attenuated. This equation includes two terms: the convergence effects (first term) and the frictional effects (second term) [16]:

$$\frac{dH}{dx} = 0.5\,(\beta + \gamma)H - \frac{f\hat{u}^2}{3\pi g\, h\, \cos\varphi} \qquad (1)$$

where H=tidal range (m), x=horizontal coordinate(km), β=width convergence coefficient (1/m), γ=depth convergence coefficient (1/m), û=peak tidal velocity along channel (m/s), h=channel depth(m), φ = phase difference between horizontal and vertical tide (degrees), $f =$ friction coefficient (unitless). If the first term (depth and width convergence effects) is greater than the second term (frictional effects), then the tidal range will increase as the channel converges [15], [16]. This tidal range amplification is usually the case in long, deep converging channels. In shallow converging channels, bottom friction generally dominates over the convergence effects. This results in a dampened tidal amplitude [16].

Tidal wave reflection is another factor in the variation of tides in estuarine systems. Reflection in closed-end channels forms an apparent standing wave [16], [17], [25]. This standing

wave occurs when the incoming tidal wave is reflected and superimposed with a second incoming tidal wave. Given full reflection, the tidal amplification can be described as [2]:

$$\alpha = \sec(kL) \quad (2)$$

where α=tidal amplification, k= wave number (1/m) and L= length from the closed boundary to the open, ocean-forced mouth (m). This type of amplification is observed in the South Bay of the San Francisco Bay [2]. Frictional forces reduce the amplitude and modify the frequency of the peak resonance [17], [25].

River flow generally dampens tidal energy as tides travel upstream. Tidal dampening from freshwater discharge occurs mainly through friction [12], [23], [26]. For long rivers without a reflective boundary, freshwater discharge dominates tidal energy. In the upstream portion of an estuary, riverine discharge begins to become more important than the oceanic tidal forcing when evaluating water level variability [26]. Eventually, tidal processes lose all influence on water levels as the dominant frictional processes deplete the tidal energy completely. River flow effects not only dampen tidal energy, but also shift the timing of high and low waters. High waters occur earlier, and low waters occur later. The low water timing is more sensitive to river discharge than the high-water timing and is prone to change more during high discharge [13].

Tides in estuaries can also be affected by channel dredging. An increase in channel depth decreases the bed friction. This decreased bed friction increases the tidal range upstream [27]. However, channel deepening can also decrease mean water levels [27], [28], due to the decrease in the surface slope needed to drive river flow downstream. Depending on whether tidal change or river slope change dominates, tidally-affected extreme water levels can either decrease or increase.

2.1.3 River Flow in Estuaries

River flow, in its simplest form in a uniform channel, is expressed by Manning's Equation. Mannings equation (Eq. 3) is a balance between the force of gravity and the opposing force due to bed stress[29]:

$$Q = VA = \frac{1.00}{n} AR^{\frac{2}{3}}\sqrt{S} \quad (3)$$

where Q= flowrate (m^3/s), v=water velocity (m/s), A=flow area (m^2), n= Manning's Roughness Coefficient, R= hydraulic radius(m), and S= channel slope (m/m). This equation assumes uniform flow conditions and the bed slope is equal to the surface slope. However, when considering tidal interaction with river flow, surface slope depends on both river currents (discharge) and tidal velocity, and is defined as follows (Eq. 4) [27]:

$$\frac{\partial z_r}{\partial x} \sim 1.36 \frac{C_d Q_R U_T}{gbh^2} \quad (4)$$

where the left hand side represents the water surface slope (m/m), C_d= drag coefficient (dimensionless), Q_R = river discharge (m^3/s), U_T=tidal velocity(m/s), g=gravitational acceleration (m/s^2), b=channel width (m), and h=water depth (m). The tidal velocity varies throughout the spring-neap tidal cycle, causing surface slope to vary.

As illustrated in section 2.1.2, river flow plays a significant role in the upstream propagation of tides. River flow also affects salinity intrusion and water levels in estuaries. Salinity intrusion occurs because of the dispersion associated with tidal motions and baroclinic exchange flows [30]. River flow transports salt downstream, out of the estuary. These two processes balance, with the net salt flux changing whenever flows or tides change [30]. Depending on tidal and river flow conditions, estuaries can become stratified, reducing vertical mixing within the water column and the effective friction [31]–[33]. The circulation induced by bottom salinity intrusion is also balanced by a (usually small) surface pressure gradient. Because the Delft3D model used in this thesis (see section 3.1) is depth-averaged, effects of salinity intrusion on water levels are not modeled. The degree to which this may impact results is assessed through evaluation and comparison of in-situ vs. modeled water levels.

2.1.4 Wind Effects on Water Levels in Estuaries; Setup and Seiching

Wind setup is the tilt of the surface of water due to strong wind in a single direction along a long fetch of a lake or estuary. This effect is temporary and returns to undisturbed equilibrium once the wind subsides. Equation 5 describes wind setup in idealized conditions [34],

$$S = \frac{nFT_s}{\rho g d} \quad (5)$$

where S=wind setup (m), n=ratio of top and bottom shear stresses, F=fetch length (m), T_s=water surface shear stress (N/m^2), ρ= water density (kg/ m^3), g=acceleration due to gravity (m/s^2), and d=water depth (m).

Since natural bodies of water almost never have uniform geometries and dynamic wind velocities and magnitudes, this equation is not practical for estuarine applications. One approach is to estimate n and T_s values as functions of wind velocity, which leads to the so-called Zuider Zee formula (Eq. 6) [34]:

$$\xi_p = \frac{V^2}{1400z} F \cos A \quad (6)$$

where ξ_p =wind setup (ft), V=wind velocity (mi/hr), z=average lake depth (ft), F=fetch (mi), A=angle between wind direction and fetch (degrees), and an empirical value with the units of mi^3/(ft*hr)^2 (=1400). In a study of Lake Champlain, the largest average wind setup height was recorded to be 0.11 meters over 19 hours of wind [34]. The maximum wind setup height for this event peaked at 0.27 meters. Lake Chaplain's fetch is roughly 85,000 m, taken on the N-S axis. For reference, the fetch from the South San Francisco Bay to the San Pablo Bay is 65,000 m. Using the Zuider Zee equation, Loiselle et al. (2021) successfully forecasted setup-induced water levels 72 hours in advance [34]. A wind setup is also accompanied by set-down. Set-down is the negative surge that occurs on the windward side of a basin experiencing a wind-induced setup. This set-down or negative surge is also known as a blowout, and it can cause significant damage for the maritime industry and is a cause for concern for boating safety in harbors. Blowouts (set-downs) often have near-symmetry regarding the magnitude when compared to the respective setup height [35].

A seiche is a standing wave that is initially formed by a perturbation on a resting body of water such as a lake or estuary. A restoring force then overshoots the resting equilibrium position, causing the system to oscillate until friction eventually damps out all motion. In this study of the SFBD, the initial perturbation is wind. The restoring force is gravity, pulling water back to

horizontal equilibrium. The longest natural period of a seiche is a characteristic of the body of water and is associated with the fundamental frequency of the water body itself. Knowing this value is crucial to understanding and predicting seiche behavior. It can be calculated with Equation 7, Merian's formula:

$$T = \frac{2L}{\sqrt{gh}} \tag{7}$$

where T=longest natural period (s), L=length of water body (m), H=average depth of water body (m), and g=gravitational acceleration (m/s^2) [36]. This equation is simplified to a rectangular basin and is only applicable in basins with relatively simple geometries. To calculate the period of more complex basins requires incorporating the effects of shape and bathymetry differences as well as the Coriolis effect [36]. For some context of seiche frequency time scales, the period of a seiche in an intertidal flat in the Central San Francisco Bay was found to be 500-1000 seconds, with a median duration of wind events equal to roughly 3 hours [20]. Increased water levels due to seiches are harder to predict than tides because of the irregular nature of wind magnitudes and directions [37].

2.1.5 Compound Events

A coastal "compound event" is a combination of oceanographic, meteorological, and hydrological processes leading to a significant impact, often due to the interaction between the processes [38]. The complex interactions between riverine and tidal forcings is a prime example of a compound event. River flooding is most important far from the coast, whereas coastal tides and storm surge are most important near the coast. In between, a region occurs in which hydrological and oceanographic processes superimpose, but also interact nonlinearly, thus impacting water levels in a spatially variable way. For example, increased riverine discharge can cause tidal amplification, attenuation, or both in an estuary [39]. Similarly, tides and surge interact with the river flow to raise mean water levels [27]. Because riverine effects on tidal amplification and dampening are spatially variable in complex estuaries such as the SFBD, accurate hydrodynamic models are one approach to evaluate how future sea-level rise and hydrological

changes will impact inundation on coastlines. Moftakhari et al. 2019 [40] outlines the need for statistical analysis and hydrodynamic modeling to estimate extreme water levels and flooding impacts more robustly.

The effects of river flow on estuary and tidal river extremes is often unclear, because of competing effects [27], [28], [41]. River flow raises tidally averaged water levels, but also increasing the frictional damping of tides and storm surge. This either leads to lower or higher water levels, depending on whether the raised water levels or increased frictional dampening is dominant at a given location [27]. As a result, river flow can potentially raise or lower the flood levels, depending on the location in the Bay and Delta [2]. In San Francisco, modeling efforts have shown the combined effect of natural variability in mean monthly sea level anomalies, storm surge, and sea level rise have the potential to increase flooding events well beyond what has been observed so far [42].

2.1.6 Salinity in Estuaries

Density effects due to salinity are relevant in the discussion of estuaries because dense, saline ocean water collides with less dense, river freshwater in these systems. This consideration is important both for practical and modeling applications. If estuary water becomes too saline, water quality issues will arise and negatively impact marine life.

From a hydrodynamic modeling perspective, considering water density stratification may lead to a more accurate representation of observed conditions. Density stratification reduces turbulent kinetic energy and the shear stress at the bed, partially decoupling the overlying flow from the bottom, and therefore decreasing frictional effects. In a depth averaged modeling approach, if the friction coefficient (C_d) was not greatly reduced, the model performed poorly in estimating tidal amplitudes upstream [31]. Using a depth-averaged, barotropic model was suggested as a source of error during extreme storm events in a numerical model of the Lower Columbia River Estuary. To account for this, modeled Chezy coefficients were adjusted based on discharge coefficients in a depth-averaged model [41]. This can be attributed to the greater stratification during high river flow [30]

Three-dimensional models account for salinity and attempt to capture the density stratification effects. In Peng et al 2014 [43], a Finite Volume Coastal Ocean Model (FVCOM) was outlined. Amplitudes and epochs of the eight major tidal constituents agreed closely to the observed conditions. However, water levels and salinity showed strong disagreement [43]. The open boundary harmonic constituents were artificially reduced by 5% to improve water level results.

2.1.7 Harmonic Analysis

In classical harmonic analysis, the tidal forcing is modelled as the sum of a finite set of sine waves with specific frequencies [44], [45]. Together, these sine waves represent the astronomical forcing of the sun-moon-earth system on tides. A least squares fit is used to determine a relative phase and amplitude of each frequency. Each different sinusoid is referred to as a tidal constituent.

UTide is a unified tidal harmonic analysis (and prediction) framework, using Matlab [46]. It is based on the work of t_tide [44]. Two main Matlab functions are used in the analysis of observed data from tidal gauges. The function ut_solv() allows for the user to input a time series of water levels, and the outputs are the major tidal constituent amplitudes and phases. Mean water levels can also be determined with this framework. The function ut_reconstr outputs a tidal prediction based on the output constituents from ut_solv and the desired times. Using these tools, it is possible to estimate tidal water levels in the past, present, or future. An ordinary least squares regression method is used to estimate coefficients in the regression equations, and additional uncertainty evaluation was introduced since t_tide. U_tide is also capable of running harmonic analysis for multiple modeled or in-situ data sets with a single execution of the function.

A drawback to the theoretical foundation that UTide utilizes is that it is recommended to use a time series of one year or less [44]. The effects of small satellite constituents, which influence major constituents like M2 or K1 over the 18.6 year nodal cycle, are assessed using idealized astronomical forcing [8]. However, in estuaries, frictional effects often reduce this nodal effect [22]. One way to adjust for nodal cycle effects is through the construction of an admittance

[4], based either on a reference gauge or astronomical forcing. Classical harmonic analysis assumes that the modulation of perihelion is effectively constant due to the slow rate of change over the 21,000-year cycle [44].

There are assumptions that can be made to still resolve the tidal constituents with a much shorter time series. Not all constituents are necessary, and eliminating redundant ones can decrease the overall accuracy. In regard to which constituents are used, tidal constituents can either be inferred, omitted, or kept. For a constituent to be inferred, there must be auxiliary information. UTide can incorporate exact times in nodal corrections, in calculation of Greenwich phases, and in the inference of constituents [46].

Constituent selection can be performed to remove constituents that are not independent from other constituents or are insignificant [46]. The Rayleigh Criteria is used to determine whether constituents are independent from one another. The conventional Rayleigh Criteria (R^R) is defined by Equation 8 [46]:

$$R^R(q_1, q_1) = \left(\frac{LOR_e}{\frac{1}{\left|\omega_{q_2} - \omega_{q_1}\right|}} \right) \Big/ R_{min} \geq 1 \tag{8}$$

where $q_{1,2}$ = chosen constituents, LOR_e =effective length of record, $\omega_{q_{1,2}}$= frequencies of chosen constituents, and R_{min}= a minimum threshold (usually R_{min}=1). R_{min} can be increased to conservatively omit more constituents. If a constituent pair does not meet the Raleigh criterion (≥1), then it is omitted from the harmonic analysis.

A signal-to-noise ratio (SNR) is used to determine the significance of a constituent with respect to noise in the raw input data, defined by Equation 9 [46]:

$$\frac{L^{smaj^2} + L^{smin^2}}{\sigma^2_{L^{smaj}} + \sigma^2_{L^{smin}}} \geq SNR_{min} \tag{9}$$

where SNR_{min}=minimum threshold value (usually SNR_{min}=1), $L^{smaj,smin}$= semi-major and semi-minor axis lengths of an individual constituent velocity vector tip (ellipse parameters), and σ_L^2 $_{smaj,smin}$= variance of the ellipse parameter. Simply put, this equation is the squared ratio between

the amplitudes and error in amplitude. Similar to determining the independence of a constituent, a larger minimum threshold value may be used to neglect marginally significant tidal constituents.

2.2 San Francisco Bay and Sacramento-San Joaquin Delta (SFBD)

While the Sacramento-San Joaquin Delta is covered in this section, the primary focus is on the San Francisco Bay, spanning from the South Bay to the Suisun Bay. This section covers the generalized site characteristics, as well as the history affecting the hydrodynamic properties of the SFBD.

2.2.1 Site Characteristics Overview

San Francisco Bay is the largest bay on the California coast and is one of the largest estuaries in North America with an area of 1,240 km^2 [47]. San Francisco is considered a bifurcated, mesotidal estuary [2]. A mesotidal estuary is an estuary that exhibits a tidal range of 2-4 meters [48]. Bifurcation refers to an estuary that splits into one or more separate paths. Study of the bay was limited until the early 1950's when pollution and water management were identified to produce negative effects. However, the San Francisco Bay has one of the longest continuous tidal records on the Pacific Ocean, with data dating as far back as 1854 [49].

The San Francisco Bay is characterized by broad shallows with relatively deep, narrow channels cut into the bathymetry. These channels range from 110m deep (at the Golden Gate Bridge) to 27m deep (at the Carquinez Strait) [47]. The bay is separated by narrow stretches of water into four smaller 'sub-bays'- the South Bay, Central Bay, San Pablo Bay, and Suisun Bay (Figure 2.1). The narrowest 'pinch point' is 800 m wide, at the Carquinez Straight, separating San Pablo Bay and Suisun Bay [50]. The Alfred Zampa Memorial Bridge spans the Carquinez Strait at the narrowest point.

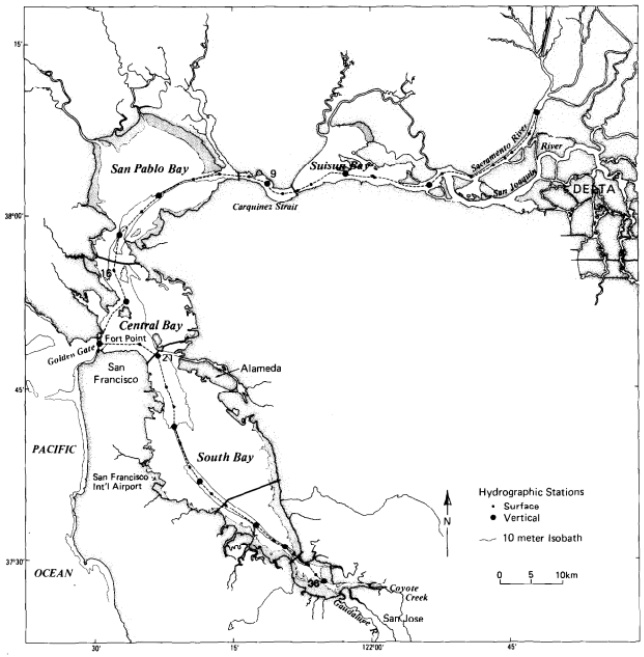

Figure 2.1: Map of San Francisco Bay and Sacramento-San Joaquin Delta with labelled sub-bays [47]

2.2.2 Historical Changes to the Bay and Delta

Sediment deposition and land reclamation drastically changed the San Francisco Bay in the late 1800s. Large scale hydraulic gold mining in the Sierra Nevada Mountains caused over 850 million m^3 of sediment to discharge into the San Francisco Bay. Between 1856 and 1887, an additional net 350 million m^3 of sediment was deposited in the San Francisco Bay [51]. During this period, three of the largest historically recorded floods aided the movement of sediment into the San Francisco Bay [4], [51], [52]. These sediment influxes caused a seaward migration of the Bay shoreline and formed large intertidal flats and tidal marshes [51]. From 1849-2011, an estimated 1,500 million tons (±400 million tons) of sediment has been delivered to the San Francisco Bay [52]

The deep channels that span the entire San Francisco Bay were naturally formed, but some portions have been dredged and straightened for shipping [10], [53]. For example, the navigational dredging of Oakland Harbor and 17 other sites in the Central Bay removed around 70 Mm^3 from 1931 to 1976 [51]. The US Army Corps of Engineers (USACE) regularly dredges

the channels in the Bay and Delta regions to maintain safe shipping passageways [54]. Roughly 3 million m^3/year of sediment is removed from navigation channels and other maintenance projects in the Bay. This removed sediment is permanently removed from the San Francisco Bay through deep-water disposal or is deposited in wetlands and other beneficial reuse projects [51]. Dredging changed the tidal prism and likely produced changes in tidal circulation and amplitudes [3], [10]. Estimates of sediment removal and deposition throughout the San Francisco Bay are highlighted below (Figure 2.2).

Figure 2.2: Bathymetry changes in the San Francisco Bay since the 1940s [51]

The Sacramento San Joaquin Delta has been heavily modified and influenced by the agricultural activities in the region. Since the late 1800s, levee construction and marshland draining have been widespread. Because of this, the Delta is a large network of both natural and artificial channels. The channels surround levied agricultural plots that often face subsidence issues and are vulnerable to high river flow events, saltwater intrusion, and sea level rise [51].

2.2.3 Future changes

There are many environmental factors that are predicted to cause hydrodynamic and ecological issues in the San Francisco Bay. Sea level rise will cause the frequency of extreme water levels to increase exponentially [55]. Sea level rise will cause decreased frictional effects in the bay and higher rates of flood inundation [2]. The modification of wetlands and marshlands may have lasting effects on the climate resilience of SFBD. Coastal wetlands and tidal marshes were shown to aid in the dampening of tidal energy and therefore decrease the effects of inundation [2]. However, the survivability of marshes under sea-level rise and altered salinity is unknown [56]. This ecosystem service of tidal dampening properties may lose effectiveness, compounding the future effects of climate change. Measurements have witnessed a 30% decrease in river discharge in the San Francisco Bay, but model projections predict larger extreme runoff events to double in frequency within the next century [57]. Moreover, the 18.6 year and 4.4 year cycles in tides influence flood risk such as the 0.01 annual exceedance probability event [58]. The estimated long-term relationship between increased extreme water levels and long-term (4.4 and 18.6 year) tidal cycles are shown below (Figure 2.3) [58].

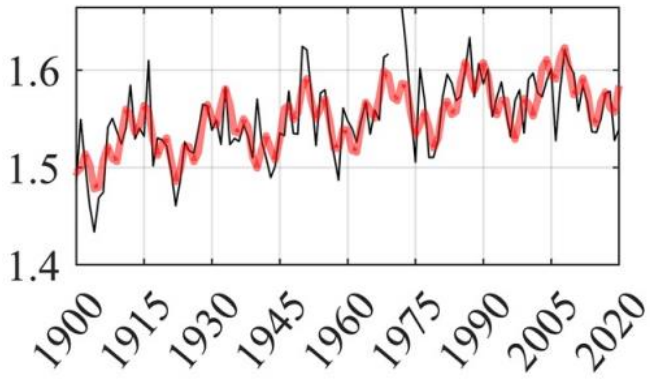

Figure 2.3: Annual 100 year extreme sea level (black) and harmonic analysis using 4.4 and 18.6 year periods (red) in San Francisco [58]

The effects of long-term tidal variations increased potential floods by 12.9% in San Francisco [58]. Subsidence and other sources of vertical land motion (VLM) (e.g. glacial isostatic rebound, soil compaction, tectonic activity) in the San Francisco Bay can have a net effect in

either up or down direction and will impact flooding in the future. Not accounting for local land subsidence in areas of the San Francisco Bay can underestimate the flood risk by up to 90.9% [59].

2.2.4 Tides in the San Francisco Bay

Tides vary greatly within the San Francisco Bay and extend far into the Sacramento-San Joaquin Delta. The Golden Gate strait is the only inlet linking the estuary to the Pacific Ocean. The tidal flow is roughly 8 x 10^9 m^3/day [51]. These tidal flows outweigh the freshwater discharge by one to two orders of magnitude [51]. The San Francisco Bar is an underwater ebb-tidal delta that spans 175 km^2. The great diurnal tidal range at the Golden Gate Bridge is 1.78 m (Mean Lower Low Water (MLLW) – Mean Higher High Water (MHHW), 1983-2001 Tidal Epoch) [51]. Ocean swell waves entering the inlet only significantly affect exposed portions of the Central Bay [51]. The tides in the South San Francisco Bay are close to a standing wave [2]. The tides travel through the Sacramento-San Joaquin Delta as far upstream as Sacramento, 180 km from the coast [3]. They eventually are damped completely by the various effects covered in section 2.1.2.

2.2.5 River flow from the Sacramento Delta

The two major rivers that feed the San Francisco Bay are the Sacramento River and the San Joaquin River. These rivers feed through an inverted delta shape, also known as a bay-head delta, that characterizes the Sacramento-San Joaquin Delta. Both rivers and their tributaries eventually feed through the Carquinez Strait. The annual mean freshwater discharge rate is 800 m^3/s and the largest recorded outflow from 1929-present is 17,800 m^3/s. The Sacramento River is the largest contributing river to freshwater discharge within the Delta, with an average flow of 550 m^3/s [57]. The Net Delta Outflow Index (NDOI) is the regulatory representation of Net Delta Outflow (NDO). NDO is estimated by performing a water balance at Chipps Island, with NDOI computed and reported as a yearly Dayflow report [60]. These QA/QC'd values, along with new flow through the Delta Cross Channel and Georgiana Slough, net flow at Jersey Point (QWEST), and the position of X_2 (2 ppt salinity isohaline) can be retrieved from the California Department of Water Resources [60].

River flow from the Sacramento Delta strongly contributes to the salinity variability from month to month. This freshwater flow is the most significant single contributing factor to water quality in the San Francisco Bay due to its effect on the salinity field throughout the estuary [56]. The watershed that drains into San Francisco Bay is 140,000 km^2 (Figure 2.4) [56].

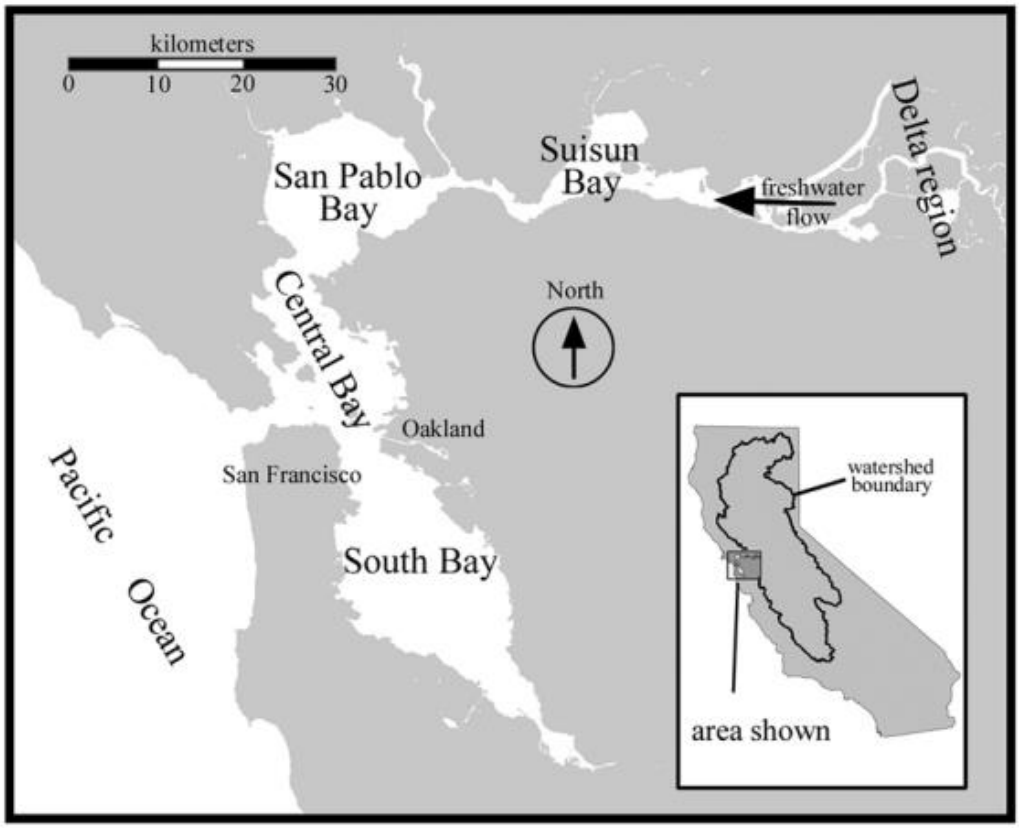

Figure 2.4: Map of the San Francisco Bay and California, displaying scale of the San Francisco Estuary's watershed boundary [56]

Natural forcing, reservoirs, and delta pumping (withdrawals) create a seasonal salinity cycle, as well as large year to year variability. Freshwater withdrawals average 6 km^3 per year, with a total storage in the watershed's major reservoirs of 35 km^3 [56]. These withdrawals are for municipal, agricultural, and industrial uses. This creates a difficult environment for fragile, newly restored wetlands to survive and recuperate in. Management of the delta also exhibits large month to month and year to year variability. During high flow years, management has less impact on the system, with the greatest impacts being during moderate flow years. Because of this, the

large natural interannual variability will cause a large interannual signal in the estuary regardless of management efforts [56]. During high flow events, like in 2017, releases from the Yolo Bypass can account for 50% of delta inflow [10]

River flow affects mean water levels in the San Francisco Bay and Sacramento-San Joaquin Delta. Median river flow causes water level variation of 0.01-1.3 m, while summertime delta pumping causes water level decreases as high as 0.35 m [57]. River flow is the most dominant factor for water level variation and MWL in the eastern Delta, but loses influence towards the west, oceanside portion of the Bay [57].

2.2.6 Wind in San Francisco

Throughout the entire year, westerly winds have the highest percent frequency reported at San Francisco International Airport from 1992-2002 [61]. When storm cyclones travel past the San Francisco Bay, their rotation brings southerly winds along the fetch of the South, Central, and San Pablo Bays. Strong southerly wind events are characteristic for winter [10], [62]. Wind can have a large effect on water levels in California. During major winter storms, onshore winds combined with low barometric pressure can lead to storm surges up to 3 ft above predicted sea levels [63]. This low pressure effect is known as the inverse barometer effect (IBE). Because southerly winds occur more often during storms, their potential to interact with small creek flow may increase the likelihood of flooding along areas where creeks meet the San Francisco Bay [20], [64].

2.2.7 Salinity in the San Francisco Bay

Salinity in the San Francisco Bay varies spatially and temporally. The distance in which the ocean salinity reaches upstream from the Golden Gate Bridge (denoted as X_2 in km) has been defined as where the bottom salinity is equal to 2 psu (practical salinity unit) [30]. During periods of high river flow, the saline water is carried out towards the Golden Gate Bridge. During periods of low flow, the salinity reaches farther upstream. Through longitudinal dispersion, tidal motion also has the ability to transport saline water upstream. The X_2 was found to range from roughly 40km near the Carquinez Strait to 95km near Rio Vista. X_2 was found to be proportional

to river flow to the 1/7 power, straying from the theoretical value of 1/3, possibly due to the increased stratification accompanying high river discharge [30]. The US Fish and Wildlife Service established a standard for X_2 =80 km or less in September and October during “above normal” and “wet” years to ensure the health of native fish and endangered delta smelt [65]. Operation of various channels and gates helps achieve the goal of keeping salinity at a suitable range. The Northern reach of San Francisco Bay (from San Pablo Bay through the Carquinez Strait to Antioch) exhibits a partially mixed or weakly stratified estuary, except during high flow events However, the horizontal density gradient is persistent in the San Francisco Bay and is relatively insensitive to riverine discharge [30], [66].

2.3 Prior Modeling Efforts of the San Francisco Bay

This section highlights previous hydrodynamic modeling efforts of the SFBD. This section covers models from the last 10 years and is not exhaustive. A common theme is a focus on the Northern reach of the San Francisco Bay, and an exclusion of the Sacramento-San Joaquin Delta. Many of these modeling efforts also seek to pair the hydrodynamic portion of the model to biogeochemical models, investigating water quality issues in the San Francisco Bay.

2.3.1 Holleman and Stacey 2014 [2]

This hydrodynamic numerical model sought to investigate how multiple shoreline scenarios in the South and San Pablo Bay respond to an increased mean sea level. The first scenario is a leveed shoreline, where tidal flows are limited to the present-day shorelines. The second scenario allows flooding to occur in all above sea level topography. In the case of the leveed shoreline, this increased depth increased tidal amplification. Tidal wave reflection in the South Bay also increased, and energy flux was shifted towards the shallow shoals in the San Pablo Bay. The decreased frictional effects were also seen in the second scenario, but the flooding increased tidal energy dissipation around the perimeter of the bay, with coastal flats acting as large energy sinks. Most inundation occurred around the sloughs and rivers in the bay. The energy dissipation of the newly inundated areas dominates the decreased frictional effects overall, as a decrease in tidal amplification was observed. This model displayed the potential for

tidal marshlands to protect against sea level rise through the dissipation of tidal energy, both in the marshland and throughout the San Francisco Bay Area. Inversely, the study also highlighted the potential risks of hardening shorelines in highly reflective basins such as the San Francisco Bay.

2.3.2 Peng et al 2014 [43]

This Finite Volume Coastal Ocean Model (FVCOM) sought to complement the National Ocean Service (NOS) Physical Oceanographic Real Time System (PORTS) with now/forecasted water levels and salinity throughout the South, San Pablo, and Suisun Bays (excluding Grizzly Bay). Tidal constituent skill passed all assessment criteria for both hindcast and now/forecast. An arbitrary 5% decrease of tidal constituents on the oceanic boundary was required for improved water level results. The reason for this was unknown and the study noted that further work would need to be done to analyze the dynamics behind the adjustment. Additionally, the model grid was not able to properly represent the Sacramento-San Joaquin Delta region. Inclusion of this region may improve the salinity predictions around Port Chicago and Rio Vista.

2.3.3 Martyr-Koller 2017 [7]

This modelling effort utilized the Delft3D D-Flow Flexible Mesh modeling suite to focus on developing a calibrated and validated hydrodynamic model with the ability to be linked to other models for analysis of climate and infrastructure changes in the San Francisco Bay-Delta (SFBD). Delft3D Flexible mesh utilized the three-dimensional incompressible Navier-Stokes equations to drive the model. The model performance was assessed with hindcasts of hydrodynamics and salinity characteristics and comparison to in-situ data. The model has been validated for water levels, flows, salinity, stratification, and large-scale floodplain inundation for a wide range of tidal and fluvial conditions. The modeled water salinity was consistently fresher and less stratified than observations. Agricultural runoff and evaporation were not included in the model, which may have contributed to this discrepancy.

2.3.4 Nuss 2018 [6]

This modeling effort focused on pairing the three-dimensional, finite-volume, unstructured Delft3D D-Flow Flexible Mesh model to the Delft3D D-Water Quality (D-WAQ) biogeochemical model. The hydrodynamic model ran for the water year of 2013, and was then used as an input parameter for the biogeochemical model. The hydrodynamic model inputs include tides, direct precipitation, evaporation, stormwater runoff, wastewater discharge, Delta outflow, and wind. This model also focused on primarily the North San Francisco Bay. The model overpredicts water levels upstream of the Carquinez Strait, which the author contributes to the truncated upstream Delta. Salinity prediction skill is reported as accurate, slightly biased fresh in the summer.

2.3.5 Hummel and Stacey 2020 [48]

Like the model from Holleman and Stacey 2014, this model sought to simulate different combinations of SLR and shoreline protection scenarios in the San Francisco Bay. They used a modified version of the U.S. Geological Survey Coastal Storm Modeling System (CoSMoS). This model utilizes Delft3D Flexible Mesh, utilizing a 2D, depth-averaged finite volume approach. Sea level rise was modeled by including an additional tidal constituent with zero frequency and an amplitude equal to each studied SLR scenario. Some of the modeled shoreline protection amplified the M2 tidal constituent by over 10 cm compared to existing shoreline conditions. Analyzing the change in various transects along the shoreline and how they interact with sea level rise may assist policymakers to make better decisions in the future concerning development and coastal infrastructure [48].

2.3.6 Wang 2021 [67]

This model focuses on suspended particulate matter (SPM) in Northern San Francisco Bay (San Pablo Bay and Suisun Bay) but includes the South Bay in the model domain. One goal was to evaluate how SPM affects phytoplankton growth through the influence of decreased light in the water column. The sediment transport model is a configuration of the Semi-implicit Cross-scale Hydroscience Integrated System Model (SCHISM), based on Chao et al. 2017. The biogeochemical model is the Carbon, Silicate, Nitrogen Ecosystem (CoSiNE) model. Wastewater

treatment plants in the model domain are included as nutrient sources. The sediment model simulated SPM concentrations well in the area of focus, and when coupled to the CoSiNE model, improved the biogeochemical results. The study also highlighted that SPM and chlorophyll-a concentration are strongly regulated by the spring-neap tidal cycle.

2.3.7 Nederhoff et al. 2021 [68]

This model developed upon the model by Martyr-Koller et al. (2017) but used 1D elements for tributaries in the Bay and rivers in the Delta. The Bay Area is represented by a 2DH (2D horizontal) unstructured grid. The inclusion of 1D elements allowed the model to efficiently simulate over 70 years. This study used this hindcast data of water levels to quantify the return period and values of extreme water levels in the San Francisco Bay and Delta. The average RMSE error of the water levels for the entire modeled period was 8.0 cm. This model is evaluated in this thesis, and it is further discussed throughout the rest of the paper.

Chapter 3

METHODS

This section details the methods used to develop the results of this study. The model configuration is documented in section 3.1, the model validation is described in section 3.2, analysis methods are described in section 3.3, model experiments are documented in section 3.4, and attempted model improvements are discussed in section 3.5.

3.1 Model Information and Configuration

The numerical model used in this study was run in Delft 3D Flexible Mesh (FM), an open-source hydrodynamic software created by the Dutch company Deltares. The software was made open source in January 2011. I used release 2022.02, SVN revision 73586 for all model simulation runs in this report. This thesis uses a model of the San Francisco Bay Area that was originally developed by Martyr-Koller et al (2017) and modified by Nederhoff et al (2021) [7], [68].

3.1.1 Model Assumptions and Equations

Delft3D uses the finite volume method to solve the Navier-Stokes equations for incompressible free surface flow under the shallow water assumptions and the Boussinesq buoyancy approximation [69] Both 1D and 2DH grids are coupled such that they are solved in the same system of equations. Equation 10, the Reynolds-averaged Navier-Stokes (RANS) equation, is as follows [69]:

$$\frac{\partial u_i}{\partial t} + u_i \frac{\partial u_j}{\partial x_i} + \frac{1}{\rho_0}\frac{\partial p}{\partial x_i} - \frac{1}{\rho_0}\frac{\partial \tau_{ij}}{\partial x_j} + \varepsilon_{ijk} 2\Omega_j u_k = \frac{\rho}{\rho_0} g \delta_{ij} \tag{10}$$

where u=water velocity, t=time, ρ=fluid density, g=gravitational acceleration, δ_{ij} is the Kronecker delta, ε_{ijk} is the permutation (Levi-Civita) symbol, Ω_j is the planetary vorticity, τ_{ij} are the turbulent stresses, and p= the sum of hydrodynamic and hydrostatic pressure. The Coriolis effect is expressed through the term that includes the planetary vorticity. The Boussinesq approximation simplifies the Reynolds-Averaged Navier-Stokes Equation by only accounting for variable density in the pressure term. Reynolds averaging is a technique used to separate the average flow behavior from fluctuations due to turbulence. Turbulent motions are then parametrized as a stress

term (the “Reynolds Stress”), and a turbulence closure model (zero, one, or two term) is used to help solve the problem. From the four turbulence closure models available in Delft3D, the $\kappa - \varepsilon$ turbulence model is used in the model in Nederhoff et al (2021) [68]. This model relates turbulent kinetic energy (κ) to the turbulent dissipation rate (ε).

In Equation 11, Manning’s roughness is used to define a drag coefficient, described below as

$$C_{2D} = \frac{\sqrt[6]{H}}{n} \tag{11}$$

where H = total water depth (m) and n = Manning coefficient ($m^{-\frac{1}{3}}s$). C_{2D} is then used to define the bed-shear stress. In the open water of the Pacific Ocean, friction values were calibrated to optimize tidal propagation in Nederhoff et al (2021) [68]. A majority of the domain had a Manning’s n value of 0.023 s/m$^{1/3}$, with lowered friction values from 0.023 to 0.020 s/m$^{1/3}$ in the South Bay and increased values to 0.030 s/m$^{1/3}$ in the Delta to improve the RMSE. It was hypothesized that these frictional effects were lower due to the muddier bottom in the South Bay compared to the rest of the estuary.

3.1.2 Data Sources

Several sources of tidal and river flow gauges were used to help define boundary conditions and/or validate model output. A relatively large amount of hourly water level data was available for WY2017 from various sources, including NOAA, USGS, and CDEC (Figure 3.1). It is important to note that not all tidal gauges have hourly data for WY2017 (either partially or completely). Of the 83 gauges represented, 70 gauges had sufficient data for WY2017. The USGS gauges located in the smaller tributaries often only had flow measurements. Gauges from Napa County, Sonoma County, and Santa Clara County did not have any data spanning WY2017. However, this large, compiled dataset of gauge locations throughout SFBD may aid future modeling work.

Figure 3.1: Model grid and representative gauge locations throughout model domain

One-minute frequency river flow inputs in the Delft3D model were based on Dayflow estimates and USGS streamflow observations [60], [70]. Twenty-two inputs total are used for fluvial inflow for WY2017, with their locations shown in the map below (Figure 3.2). Sixteen of the inflows were compiled from USGS and 6 are Dayflow estimates (see Section 2.2.5).

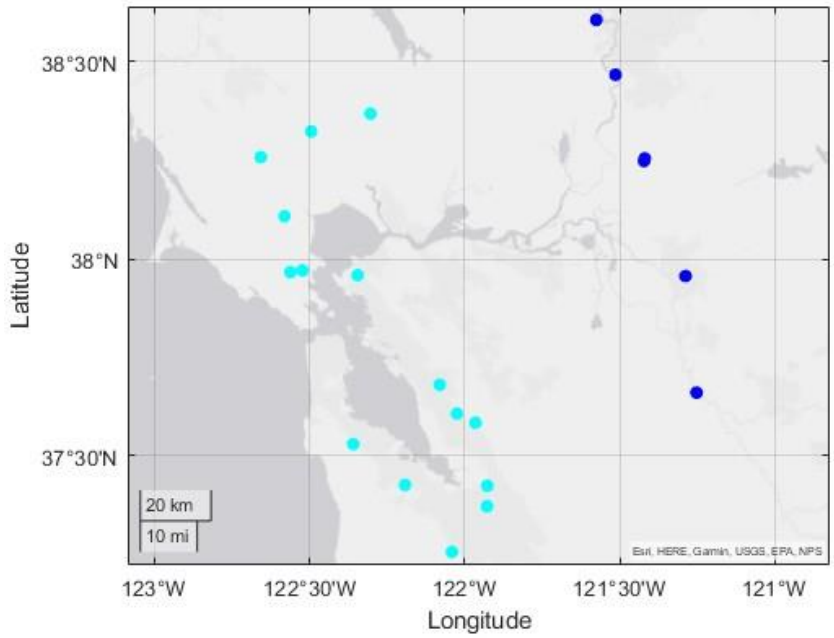

Figure 3.2: River flow input locations- cyan represents USGS stream flow gauges (16), dark blue represents Dayflow estimate inflows (6)

The sources of topo-bathymetry data for the entire model domain are from the USGS [71]. The San Francisco Bay elevation lidar data horizontal resolution is 2 m and the Sacramento-San Joaquin Delta horizontal resolution is 10 m [72].

The wind forcing that the Nederhoff study used was generated using data from ERA5 [73]. ERA5 is a fifth generation European Center for Medium-Range Weather Forecasts (ECMWF) reanalysis for global climate data and weather, spanning back to 1940. ERA5 predicts wind at a 10m height. To correct for the 10m height, Equation 12, the LLLJP Wind Shear Power Law was used and is described as [74]

$$u = u_{ref}(\frac{z}{z_{ref}})^{\alpha} \quad (12)$$

where u=mean wind speed, u_{ref}=mean wind speed at the reference height (m/s), z=10m, z_{ref}=reference height (m), and α=wind shear exponent. Nederhoff (2021) corrected the data to the same 10m height assuming a constant power law and a wind shear exponent of 0.16 [68]. The study acknowledges that the ERA5 wind forcing deviates from observed conditions at speeds

above 10 m/s and wind direction error is larger than the magnitude discrepancy. Additionally, ERA5 wind forcing is coarse, with 30km between points. In this study, in-situ wind data was compiled from 8 NOAA meteorological stations and 5 NOAA National Weather Service (NWS) stations. I corrected the values to 10m height and applied the data to the numerical model to improve the fidelity of wind forcing (See section 3.4.2).

3.1.3 Model Grid

The model grid of the San Francisco Bay used in this research (Figure 3.1) was constructed in [68]. The grid consists of 185,690 rectangular and triangular grid cells with a minimum cell resolution of 100 meters. The grid extends ~40 km offshore. Landward, the 1D model network extends into the San Joaquin River until near Vernalis (189 Rkm) and into the Sacramento River until near the outer southern suburbs of Sacramento (169 Rkm). The 2DH grid comprises a majority of the Bay. The 1D channel network used to represent the Delta is linked to the 2D grid near Antioch (94 Rkm). All DEM sources utilized have a greater horizontal resolution than the grid.

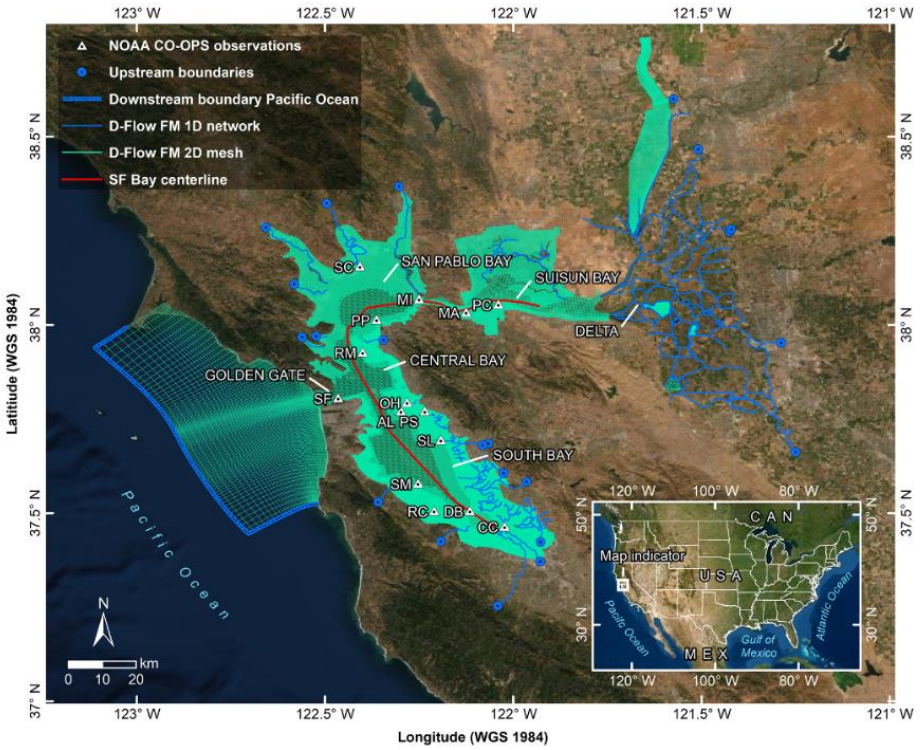

Figure 3.3: 1D/2DH model grid utilized in this study, outlined in Nederhoff et al., 2021 [68]

The purpose of Nederhoff (2021) was to simulate extreme water levels in the SFBD for nearly 70 years (1950-2019) with hourly timesteps. Therefore, efficiency was a key priority. They utilized both 1D networks and 2DH grids to achieve greater efficiency than the Martyr-Koller (2017) flexible mesh grid. The bay, permanently flooded delta islands, and the Yolo Bypass floodplain are all represented by 2DH grids. The 1D networks represent the tributaries flowing into San Francisco Bay and multiple rivers in the Sacramento-San Joaquin Delta. Replacing riverine areas represented by a 2D grid with a 1D network decreases the computational demand of simulation runs compared to a full 2D grid. Additionally, Nederhoff et al. (2021) expanded the earlier grid to incorporate the low-lying intertidal lands in the South, San Pablo, and Suisun Bays.

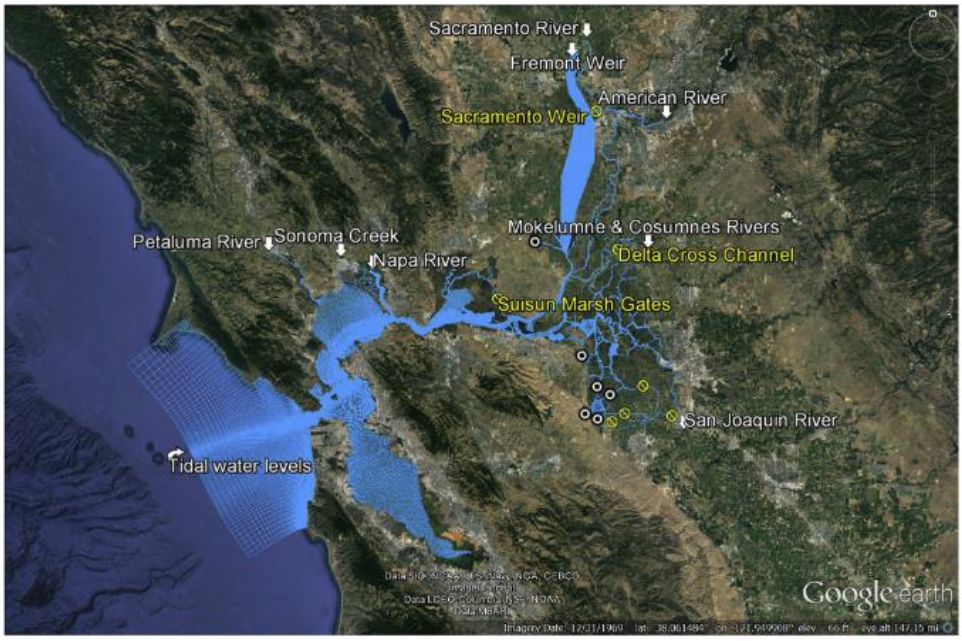

Figure 3.4: D-Flow FM 3D model grid from Martyr-Koller et al. 2017 [7]

3.1.4 Boundary Conditions

The offshore boundary tidal constituents were based on 67 tidal constituents observed at the NOAA San Francisco (Station 9414290) gauge but altered slightly. Since the tidal constituents are propagating into the model roughly 40km offshore from where they were observed, the amplitudes and phases of M2, K1, O1, S2, P1, and K2 were adjusted. The amplitudes were decreased by a factor between 0.87 and 1. The phases were increased between +4.3 and 0^{o}.

The non-tidal residual (NTR) was applied uniformly across the ocean boundary based on the NOAA San Francisco gauge. The NTR was based on the observed signal minus the predicted tide at the NOAA San Francisco gauge. A daily moving mean was applied to remove short term noise. The NTR applied includes inverse barometer effects (IBE), steric effects such as changes to oceanwater density due to differences in temperature in salinity and temperature, and sea level rise.

River discharges in the Bay Area (down river of the Carquinez Strait) in the Nederhoff et al. (2021) model are based on 16 USGS flow stations. The discharges in the Delta are based on Dayflow estimates [60]. Other models have up to 44 river and stormwater inputs [6].

3.1.5 Model Observation Points

I used observation points within the grid domain to represent water level gauges. With cell resolutions of 100m at the smallest, sometimes observation points did not well represent in-situ gauges (for example, if the cell was subject to wetting and drying). Thus, observation points were sometimes placed at the thalweg near the in-situ gauge. The use of observation points significantly reduced the memory usage required, when compared to analyzing the entire grid as a dataset. A total of 1,543 observation points were defined and utilized, reducing the amount of output data by an order of magnitude compared to the full grid. The observation set represented over 200 gauge locations from NOAA, USGS, CDEC, and local municipalities. The observation set also defined the thalweg (the deepest channel) at 1 km resolution throughout the 2DH portion of the model, through the main channels of the Sacramento and San Joaquin Rivers in the 1D portion, extending to the model boundaries. The land boundary is also represented by observation points in the 2D grid domain [68].

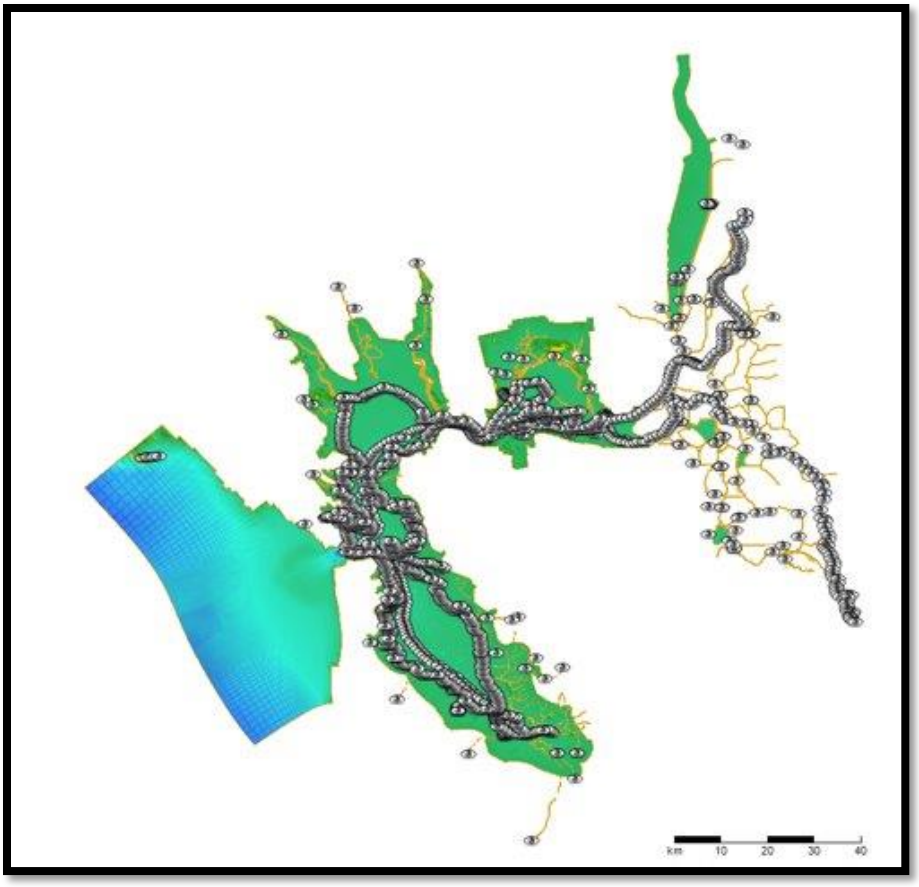

Figure 3.5: Observation points specified for analysis

3.2 Model Execution

In this study, the Nederhoff model was run and analyzed for WY2017 (October 1, 2016 - September 30, 2017). A 2-day spin-up period was also included, to avoid the non-representative effects of a “cold start” of a model at rest. WY2017 is considered a high flow year for San Francisco, breaking the record for precipitation in Northern California, set in the water year of 1983 [75]. The peak water flow events in the Sacramento River and San Joaquin River occurred in February and March of 2017. These high flow events allow us to analyze the performance of the model during both low and high flow conditions.

3.2.1 Simulation Approach

Each simulation run in this research process utilized an ASCII file with the file extension .mdu (Master Definition FLOW) as an intermediate step between the graphic user interface (GUI)

and the simulation program of Delft3D [69]. All aspects of the model are available for viewing and modification through this master definition file. From a list of model options and file path references, I could change the model grid, observation points, computational timestep, turbulent closure model, constant water density, wind drag coefficient type, start and stop times, external forcings (wind, river flow, oceanic boundary conditions), and data output frequency and format. Because of the simplicity of this .mdu file, I used it to facilitate running different experiments (covered in section 3.3) where I investigated the effect of individual forcing factors by modifying forcings individually.

3.2.2 Mean and Tidal Water Levels

Mean water levels (MWL) are variable on both daily and monthly time scales and are dependent on multiple factors such as wind, river flow, and oceanic non-tidal variability [57]. Hourly water levels were compared to the in-situ time series in regard to timing and magnitudes of the peak and trough water levels. I evaluated spatial patterns of MWL to determine where river flow drives MWL variability in the SFBD. Improper flow routing, or the exclusion of mass balance-affecting processes like evaporation and groundwater percolation can affect the model performance. Incorrectly represented frictional effects can also affect mean water levels. Bottom roughness can vary by more than a factor of three within a 2km stretch of river [76]. Considering the 100m grid resolution in the Delft3D model, analyzing the MWL may reveal inaccuracies due to the simplified modeled bottom friction. Daily mean water levels are influenced by tides on a fortnightly scale as well as seasonal scale. Wind setup from westerly winds also raises water levels inland of the Carquinez Strait by 0.03-0.14 m [57].

I compared the output hourly water levels and in-situ time series by calculating mean water levels over 32 day period. I then evaluated the timing and magnitudes of the peak and trough water levels, defining and analyzing metrics such as root-mean square error.

3.2.3 Tidal Amplitudes and Harmonic Analysis

I used UTide (see section 2.1.7) to perform harmonic analysis for both the observed and model output hourly water levels. The tidal constituents alter spatially throughout the delta, rather

than simply diminish as they travel through the estuary (Table 3.1) [77]. This effect, specifically tidal amplification in the South Bay, may change due to sea-level rise [2]. In this study, the agreement between observed and modeled M2 amplitudes was used as a metric of model performance. This agreement was analyzed throughout both the low and high river flow periods of WY2017 throughout the model domain. River flow diminishes and distorts the tidal wave [4]. By analyzing a high flow year like WY2017, the model can be evaluated on its ability to replicate the dissipation and distortion of the tidal wave during various regimes of river flow. Because it is the largest constituent in San Francisco Bay and because of its known sensitivity to river flow [4], the M2 amplitude is the main metric in this study used to analyze the spatially varying tides.

Table 3.1: Eight major tidal constituents reported at NOAA tidal gauges throughout the San Francisco Bay [77]

Tidal Constituent / NOAA Gauge	M2	S2	N2	K2	K1	O1	P1
Point Reyes 9415020	0.55	0.137	0.121	0.038	0.383	0.235	0.118
San Francisco 9414290	0.576	0.137	0.122	0.04	0.37	0.23	0.114
Alameda 9414750	0.68	0.153	0.14	0.047	0.379	0.231	0.117
Redwood City 9414523	0.885	0.201	0.179	0.064	0.404	0.238	0.126
Richmond 9414863	0.604	0.138	0.125	0.044	0.366	0.222	0.114
Martinez 9415102	0.533	0.096	0.097	0.026	0.296	0.163	0.098
Port Chicago 9415144	0.496	0.097	0.093	0.046	0.275	0.158	0.079
Rio Vista 9415316	0.369	0.066	0.068	0.029	0.221	0.111	0.082

UTide automates harmonic analysis and processes a given water level timeseries into the amplitude, phase lag, and speed of the tidal constituents [46]. UTide was used to calculate the M2 based on 32-day periods with a 1-day timestep. This approach yielded 332 estimates of M2 from October 17th 2016 to September 13th, 2017. Because of the overlapping data, sequential results are not completely independent of each other, but in practice follow weekly and monthly

variations to river flow fairly well (see Section 4.1.3). I used the ordinary least squares (OLS) method of fitting. I omitted nodal/satellite corrections. I also utilized UTide's default white noise floor assumption in the confidence interval estimate [46].

3.3 Modeling Experiments

The model experiments carried out over the period of January 30th, 2017 to March 12th, 2017 and their naming conventions are tabulated below (Table 3.2). These naming conventions will be used throughout the rest of this report. This period was chosen because it captures the large river flow events of WY2017, although many of the experiments exclude river flow. The length of this period also allows multiple fortnightly spring-neap tidal cycles to occur.

Table 3.2: Numerical model experiments performed and their attributes

Experiment	Short Name	Tides	Delta Inflow	Bay Tributary Flow	Wind Forcing
Full	WY17_Full	Full	Full	Full	Full
Base	WY17_Base	Full	300 CMS in Sacramento River	None	None
Wind 5 S Base	WY17_Base_5S	Full	300 CMS in Sacramento River	None	Constant uniform 5 m/s southerly
Wind 5 W Base	WY17_Base_5W	Full	300 CMS in Sacramento River	None	Constant uniform 5 m/s westerly
Wind 10 S Base	WY17_Base_10S	Full	300 CMS in Sacramento River	None	Constant uniform 10 m/s southerly
Wind 10 W Base	WY17_Base_10W	Full	300 CMS in Sacramento River	None	Constant uniform 10 m/s westerly
Wind 15 S Base	WY17_Base_15S	Full	300 CMS in Sacramento River	None	Constant uniform 15 m/s southerly
Wind 15 W Base	WY17_Base_15W	Full	300 CMS in Sacramento River	None	Constant uniform 15 m/s westerly
Wind 20 S Base	WY17_Base_20S	Full	300 CMS in Sacramento River	None	Constant uniform 20 m/s southerly
Wind 20 W Base	WY17_Base_20W	Full	300 CMS in Sacramento River	None	Constant uniform 20 m/s westerly
Full Wind NOAA	WY17_Full_NOAA	Full	Full	Full	Improved (see Section 3.4.2)

The WY17_Full experiment represents the as-is Nederhoff et al. (2017) model. The WY17_Base experiment represents the model system with only tidal forcing and low river flow. A net delta outflow of 300 m^3/s was chosen based on the average summertime low flow values during WY2017. I compare the results of these two simulations to evaluate the effects of river flow on water levels throughout the SFBD. The WY17_Base_XY experiments (where X represents wind speed and Y represents wind direction) add wind forcing into the WY17_Base experiment to evaluate the maximum equilibrium response of multiple wind speeds and directions. These

experiments are further outlined in Sections 3.3.1, 4.2.2, and 4.2.3. The WY17_Full_NOAA experiment keeps the tidal and fluvial attributes of WY17_Full but replaces the ERA5 wind forcing with a new forcing based on meteorological data at NOAA and airport wind gauges. Details of this improvement attempt are covered in Sections 3.4.2 and 4.2.4.

3.3.1 Wind

Eight of the eleven experimental simulations consisted of different experiments to determine the response of water level to different directions and magnitudes of wind forcing. The inverse distance weighted wind forcing discussed in section 3.4.2 was implemented in the WY17_Full_NOAA experimental model run. A wind sensitivity study was performed with the two predominant cardinal wind directions. I simulated multiple steady southerly and westerly wind conditions, to better understand/determine the influence of predominant winds during winter storms and summertime onshore wind events, respectively [10], [62]. I implemented constant windspeeds to determine a maximum equilibrium response of water levels in the model domain, similar to a study focusing on the New York Harbor [35]. Constant windspeeds of 5, 10, 15, and 20 m/s in both southerly and westerly directions were implemented over the aforementioned 42-day period (section 3.3). Identical to the full water year simulation, a 2-day spin-up period was used to prevent the model from crashing. This ramp-up period occurs before the analysis period. This prevents the data from being biased towards smaller wind magnitude effects.

3.3.2 River Flow

River flow was reduced to a steady 300 m^3/s from only the Sacramento River to isolate the effects of oceanic and atmospheric forcings in all of the Base experiments. Creek flow was removed in these as well.

3.4 Model Improvement Methods

The following section describes the methods used to attempt to improve the model. The first section covers grid refinement, and the second section covers the creation of new wind forcing based on in-situ data from meteorologic gauges throughout the model domain.

3.4.1 Grid Refinement

Based on the analysis of tidal constituents (see sections 4.1.2-4.1.4), I attempted to improve the model by increasing the grid resolution perpendicular to the direction of flow in the Carquinez Strait. This location is one of the narrowest portions of the San Francisco Bay. The narrowest portion of the strait is 800 meters wide at the Alfred Zampa Memorial Bridge. Based on the elevated decrease in constituents through the strait, I hypothesized that the low resolution of the grid was restricting water conveyance upstream. To increase the resolution of the grid, I used RGFGRID Version 6.07.00.72783. This software is part of the Delft3D suite and was accessed through the Delft3D GUI. I refined the grid at the Carquinez Strait while keeping the orthogonality as low as possible. The model did not initialize if the maximum orthogonality was above 0.300 and it experienced stability issues if the maximum orthogonality value was slightly lower than 0.300.

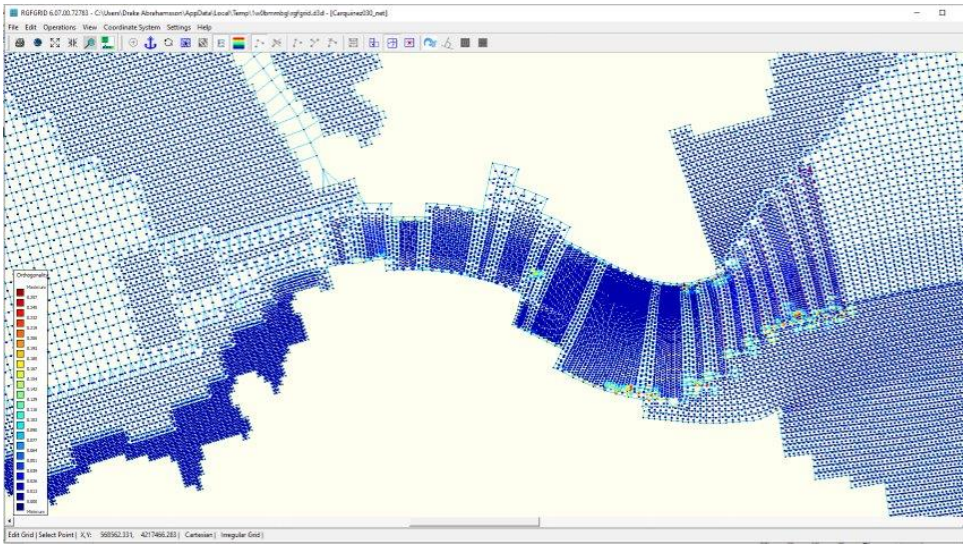

Figure 3.6: Modified grid at Carquinez Straight in the RGFGRID program, with the color scale displaying orthogonality values showing a minimum value of 0.000 and a maximum value of 0.257

3.4.2 Wind Forcing

The coarse resolution of the ERA-5 wind forcing motivated an investigation of local wind forcing, specifically to determine the influence of topography and other local meteorological

effects on the ERA5 reanalysis. By comparing the magnitude and direction of local wind measurements against the ERA5 wind forcing, I investigated whether the wind forcing utilized by the model represented actual conditions. The veracity of ERA5 wind direction and magnitude was tested against in-situ measurements by using wind roses (direction-intensity histograms) that are commonly used in the field of meteorology. I hypothesized that employing real observed local wind data rather than a reanalysis could increase the model performance because of the importance of wind direction on setup effects. Data from thirteen wind gauges for WY2017 throughout the model domain consisting of NOAA meteorological gauges and publicly available airport gauges from the NWS formed the data set (Figure 3.7). The NOAA gauges utilized were from San Francisco, Point Reyes, Port Chicago, Richmond, Alameda, Martinez, and Redwood City. The airport locations were Oakland Airport, SFO Airport, Napa Airport, Concord Buch Airport, Sacramento Airport, and Stockton Airport (Table 3.3). The wind directions and magnitudes were inverse distance weighted (IDW) between the stations and projected to the ERA5 grid (Figure 3.8).

Table 3.3: List of wind stations compiled to develop model wind forcing. Data obtained from NOAA and NWS (NOAA, NWS)from NOAA and NWS (NOAA, NWS)

Gauge Name	Gauge Number/ Identifier	Source	Latitude	Longitude
San Francisco	9414290	National Oceanic and Atmospheric Administration (NOAA)	37.80670	-122.46500
Point Reyes	9415020		37.99670	-122.97500
Port Chicago	9415144		38.05600	-122.03950
Richmond	9414776		37.92300	-122.40958
Alameda	9414750		37.77167	-122.29833
Martinez	9415102		38.03464	-122.12519
Redwood City	9414523		37.50670	-122.21000
Oakland Airport	CLIOAK	National Weather Service (NWS)	37.71780	-122.23294
SFO Airport	CLISFO		37.61962	-122.36562
Napa Airport	CLIAPC		38.20750	-122.27944
Concord Buch Airport	CLICCR		37.99167	-122.05194
Sacramento	CLISMF		38.50674	-121.49597
Stockton Airport	CLISCK		37.88972	-121.22361

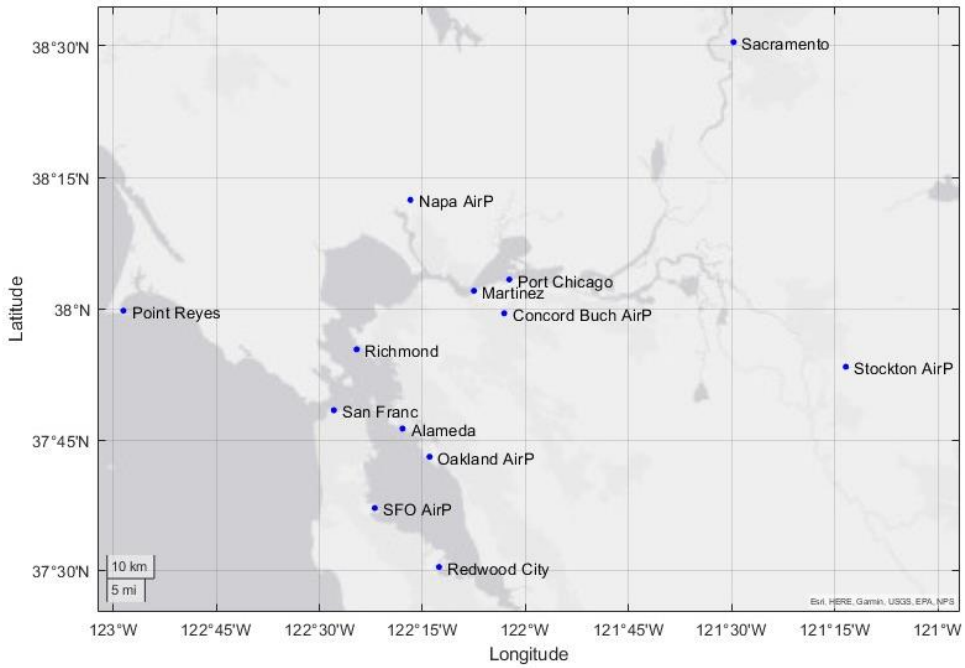

Figure 3.7: Spatial Representation of the data interpolation points in Table 3.3

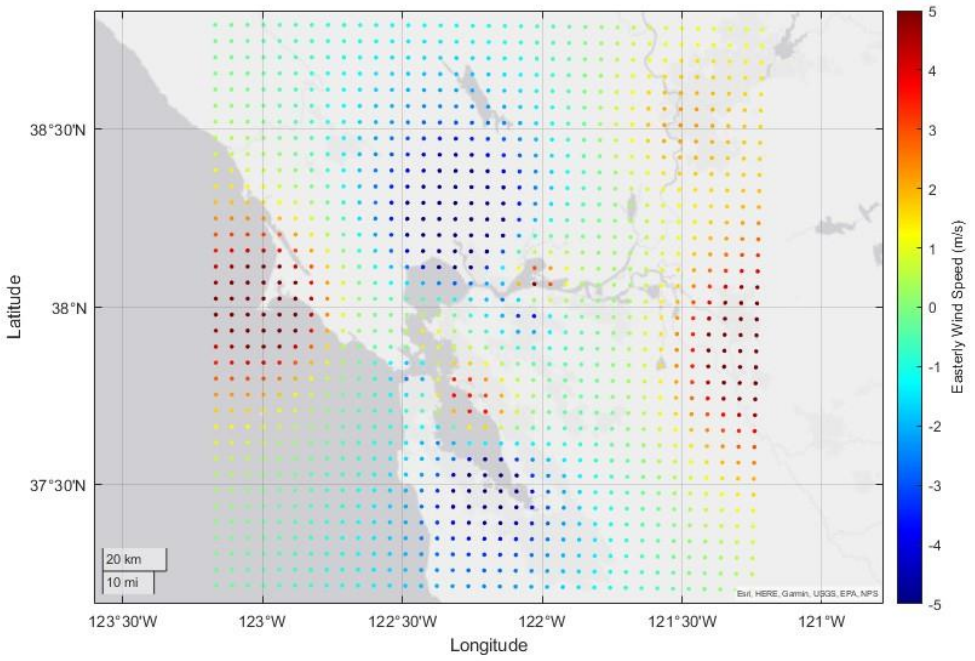

Figure 3.8: ERA5 grid, overlaid with a representative snapshot of interpolated wind data.

The new grid kept the same dimensions as the ERA5 grid for the Delft model due to software limitations (Figure 3.8). I utilized MATLAB to create a new, higher resolution grid, but the Delft model would not initialize with the increased resolution. I was however able to make a functioning grid with the new data (Table 3.3) by interpolating the NOAA/NWS data directly onto the pre-existing ERA5 grid. I utilized an inverse distance weighted approach to interpolate the wind velocity and magnitude between data points [78]. The ERA5 wind forcing in the Nederhoff et al. (2021) model included variable wind pressure. For the in-situ wind forcing model runs, I kept the atmospheric pressure constant at 101.325 kPa due to poor initial results of interpolating atmospheric pressure between data points. The influence of the inverse barometer effect is included in the non-tidal residual boundary condition at the ocean boundary [68]. Therefore, I assumed that using constant atmospheric pressure is a reasonable assumption in this experiment.

Chapter 4

RESULTS

4.1 Model Skill Assessment/Validation

This section covers the model's ability to accurately simulate tidal water levels and tidal propagation throughout the model domain. The model performance is spatially variable. An overview of representative water level and M2 amplitude comparisons between modeled and observed data is shown below (Figure 4.1). The modeled water levels and tidal signals in the complex Delta region were often less accurate than the Bay Area portion of the model. Modeled and observed water levels could be seen to consistently differ throughout the year (see Port Chicago in Figure 4.1). Modeled M2 amplitudes were more consistent, but still performed better in the Bay Area. M2 amplitudes were also underpredicted by the model in the Delta region during the low flow summer season. Overall, the model consistently displayed an ability to reproduce qualitative trends of both water levels and M2 amplitudes throughout the model domain.

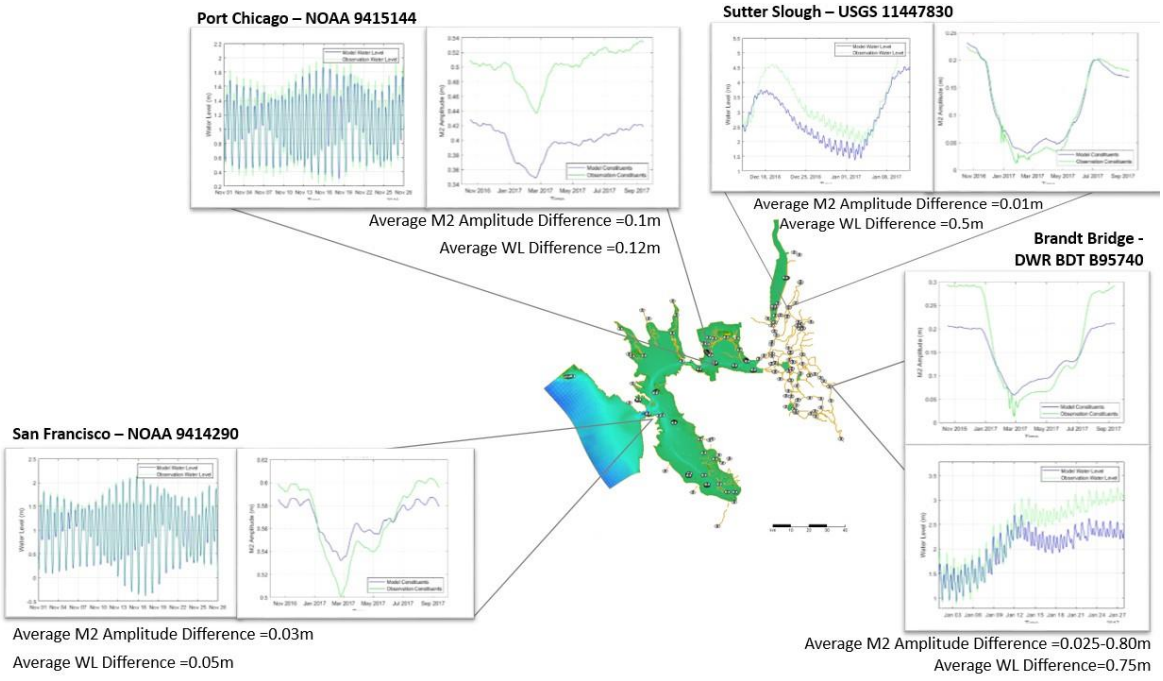

Figure 4.1: Representative water level (left) and M2 amplitude (right) time series for different regions in the SFBD; modeled values are shown in blue and observed values in green

4.1.1 Modeled Water Levels

Over the timespan of WY2017, the model captured the water level with RMSE values below 0.34m throughout the 2DH-represented Bay Area of the model, but the 1D-represented Delta region showed RMSE values as large as 1.7 m at the Yolo Bypass (Figure 4.2). A typical water level RMSE value in the Bay Area is roughly 0.1 m. In the Delta region, a typical water level RMSE value is around double the Bay at around 0.2 m. For any experiments performed with this model, I will focus more on the implications of the results in the Bay Area due to the higher accuracy of reported water levels. Among the 70 gauges with data for WY2017, only 24 had listed vertical datums. The RMSE analysis for water levels therefore only consisted of 24 gauges.

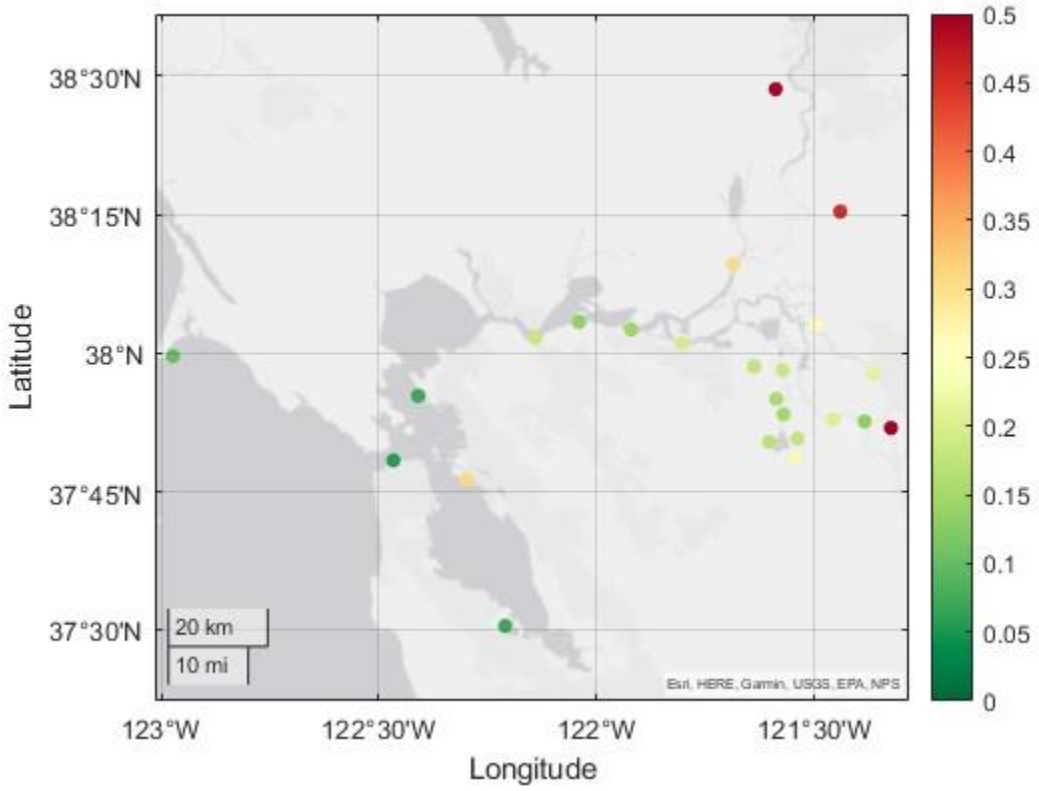

Figure 4.2: Tidal water level RMSE for WY 2017 for all gauges with known/listed datums in or converted to NAVD-88

Because of the lower accuracy in the fluvial-dependent Delta region, I investigated whether river discharge is being adequately represented in the model by comparing measured

and in-situ discharges. The model utilizes 6 DAYFLOW sources for riverine boundary conditions upstream of Chipps Island. When compared to the full set of NDOI DAYFLOW data, the sum of these 6 inputs match the NDOI during both the high and low flow periods of WY 2017 (Figure 4.3). This suggests that river flow is modeled and routed reasonably well through the delta, and the error is more likely a result of tidal or atmospheric forcing. An increase in friction (Manning's n) may help increase tidally-averaged water levels in the Delta, but would further decrease tidal range below in-situ measurements. Thus, underprediction of both mean and tidal water levels in the Delta region is caused by other factors such as the 1D idealized bathymetry. Uncertainty in river flow measurements (typically ±10%, but not reported for these gauges) may cause some additional error, though the influence on water level during low flow is likely small for San Francisco Bay and much of the Delta, given the relatively small surface slope during those conditions (see Equation 4). There are known accounting errors in the calculation of NDOI, such as the inflow from the Yolo Bypass during the summer [5]. This may be a cause of the increased error witnessed in the summer months of the simulated WY 2017.

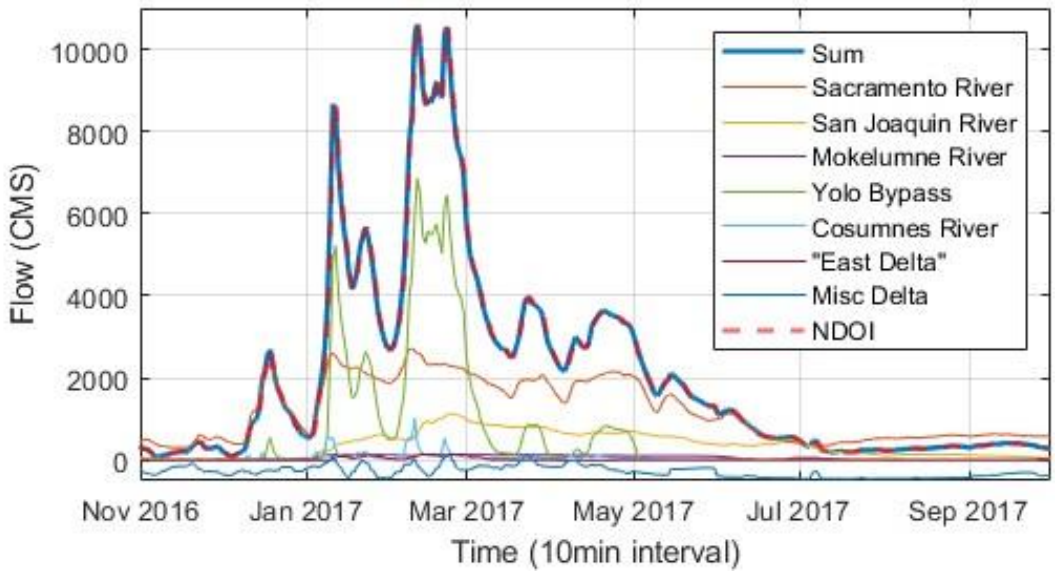

Figure 4.3: NDOI plotted against 6 riverflow inputs from Delft 3D model

The mean water level gradient during low flow (November 1-December 3 2016) stays gradual until far upstream in both the Sacramento River and the San Joaquin River with a slope

of 0.09 cm/km between the 15 km stretch between the eastern boundary of the San Pablo Bay and the Benicia Martinez Bridge. During high flow events (January 16-February 17 2017), the change is most rapid at the Carquinez Strait with a river slope of 0.5 cm/km over this same stretch (Figure 4.5). The plotted mean water level values are determined by taking the mean water level for the entire analysis periods. The tabulated values are the calculated difference between high and low flow MWL values. During high flow, the entire model domain experiences increased mean water levels, but the increase occurs at different magnitudes ranging from 0.15 to 4.1 m (Table 4.1). At San Francisco, measured mean water levels between November 2016 and February 2017 increased by ~0.15 m, consistent with model results. The difference in mean water level at Monterey (NOAA Station 9413450) for the same periods was 0.0255 m. Therefore, the majority of increased water level is likely related to local forcing such as river flow.

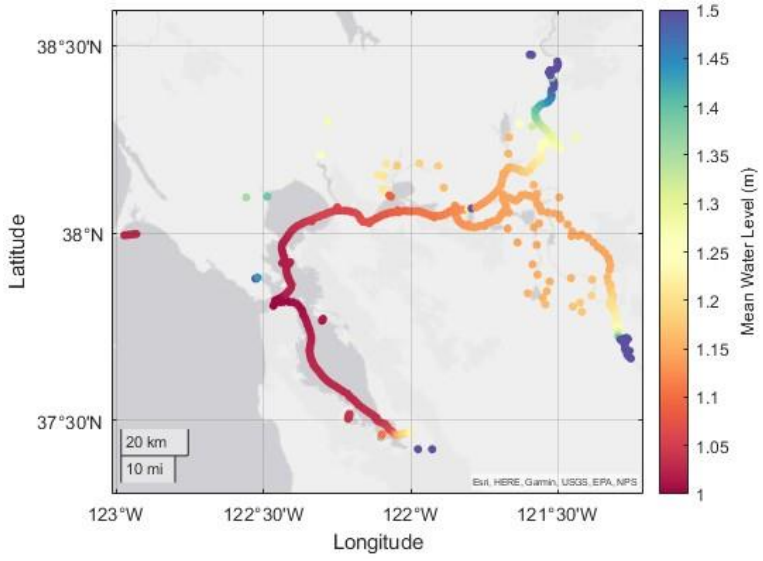

Figure 4.4: Modeled NAVD-88 MWL during low flow period (November 1-December 3 2016)

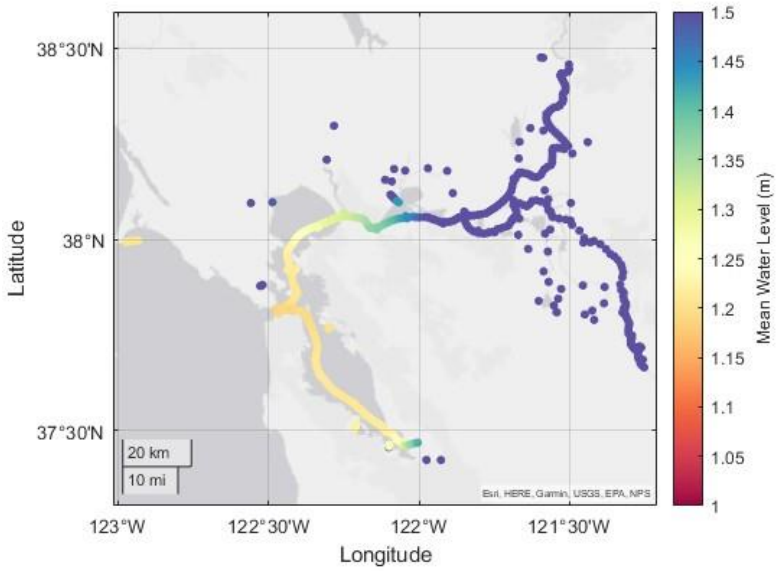

Figure 4.5: Modeled NAVD-88 MWL during high flow period with the same color scale as Figure 4.4 (January 16-February 17)

Table 4.1: Increases in mean water levels from the low flow period (November 1-December 3, 2016) (Figure 4.4) to the high flow period shown above (January 16-February 17, 2017) (Figure 4.6) adjusted for oceanographic mean water level difference (-0.0255 m) from Monterey (NOAA Station 9413450)

SFBD Region	Point Reyes	Golden Gate Bridge	South Bay	Central Bay	San Pablo Bay	Grizzly Bay	Sacramento River Model Boundary	San Joaquin River Model Boundary
Increase in MWL between low and high flow(m)	0.1559	0.164	0.1565	0.1621	0.1995	0.3195	3.9795	4.0795

The difference between low and high flow period mean water levels displays a change in mean water level of 0.156 m at Point Reyes (Figure 4.6). San Francisco was used in the model by Nederhoff et al (2021) to establish the tidal constituents at the oceanic boundary, but this location is not independent of river flow [68]. This increase in mean water level at Point Reyes is qualitatively consistent with observed conditions, but the model overpredicts the MWL increase by 0.08 m, potentially due to the use of San Francisco in establishing the tidal boundary condition.

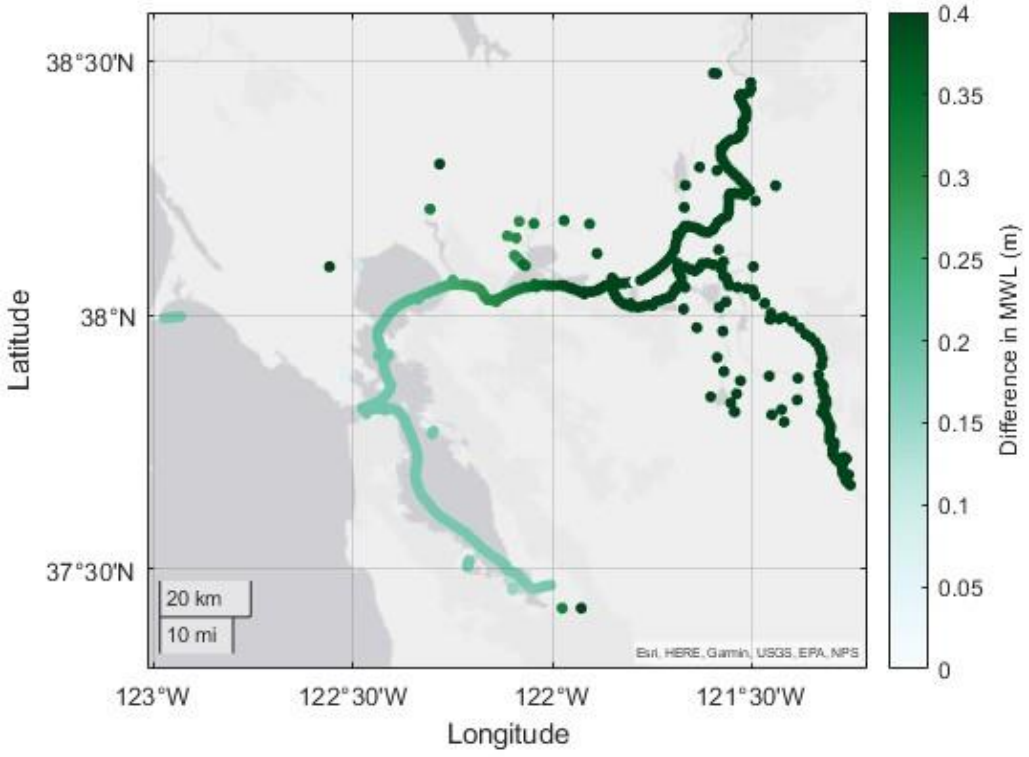

Figure 4.6: Difference in MWL from low flow period (November 1-December 3 2016) to high flow period centered on peak of flow events for WY 2017 (January 16-February 17)

4.1.2 Modeled M2 Amplitude Model Performance Throughout SFBD

Figures 4.7 and 4.8 display the observed and modeled average M2 amplitudes for WY2017, respectively. The modeled M2 amplitudes throughout WY2017 are underpredicted at nearly every observation point upstream of the Carquinez Strait, most notably directly upstream of the Carquinez Strait in Grizzly Bay. This underprediction of M2 upstream of the Carquinez Strait is also noted in the M2 amplitude timeseries (Figure 4.10). It is likely that the frictional effects of the model, particularly at the Carquinez Strait, are too high. When tidal energy is not transmitted upstream as expected, water levels and M2 amplitudes are both underpredicted by the model (Figure 4.2, Figure 4.8-4.10). Despite the underprediction of M2 amplitudes, the model still performs well throughout the model domain with the M2 amplitude RMSE values averaging 0.099 m throughout the entire model domain.

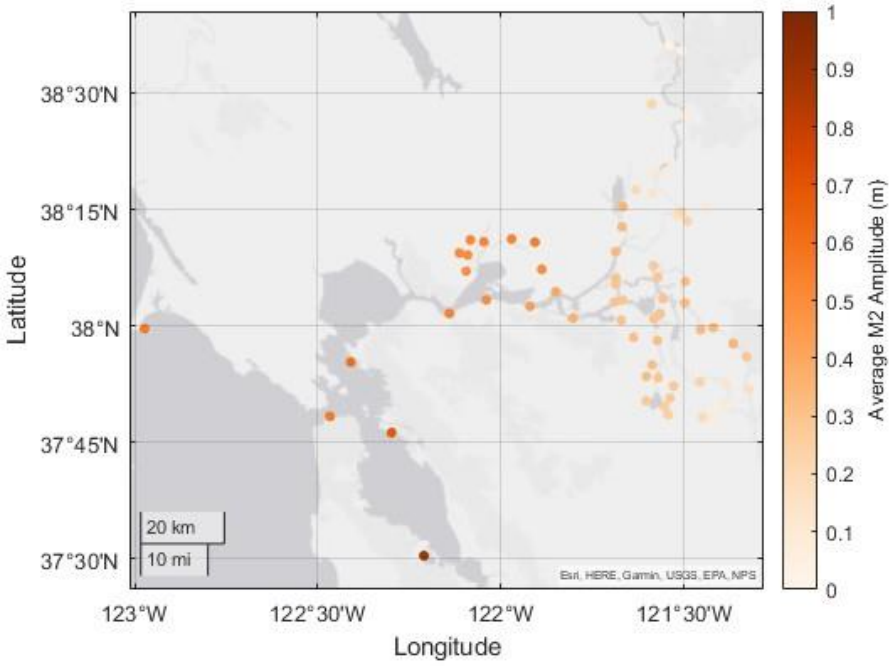

Figure 4.7: Observed yearly average of M2 amplitude for WY 2017

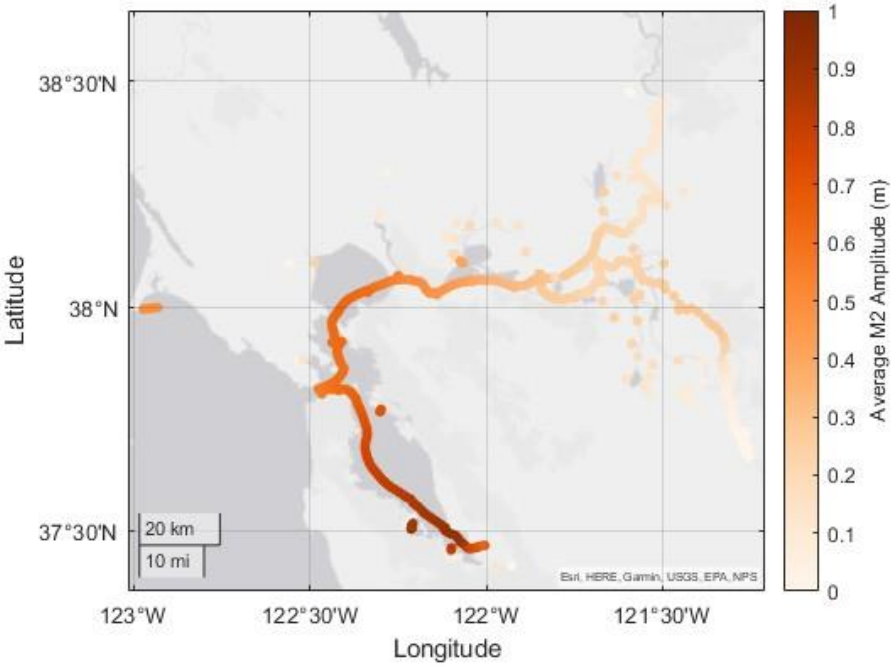

Figure 4.8: Modeled yearly average of M2 amplitude for WY 2017

Overall, the model captured the M2 well throughout both the San Francisco Bay and Delta regions, amongst the 70 tidal gauges compared. The M2 amplitude does not require a datum to compare between gauges, so I was able to use a larger portion of the initial 70 gauge dataset that spanned extensively into the Delta with data for WY2017. The exception to this good performance was Grizzly Bay. The RMSE was much larger in this region than anywhere else in the model domain with RMSE values as high as 0.5 m, while the rest of the model did not see RMSE values higher than 0.15 m in the Delta and values as low as 0.006 m at Richmond (Figure 4.10). The complex and shallow bathymetry of Grizzly Bay may be a cause of the decreased accuracy.

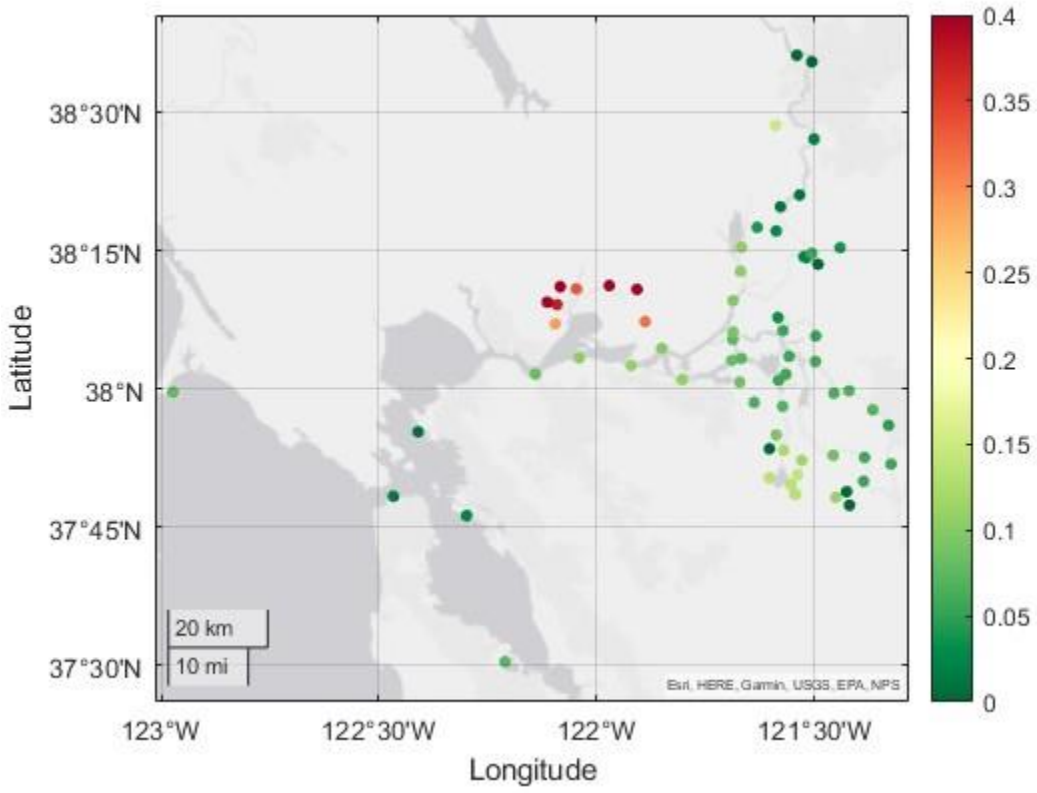

Figure 4.9: Spatially represented RMSE of M2 amplitude for entirety of WY 2017 based on 332 trials of 32 day periods

Due to the wide distribution of M2 amplitudes throughout the model domain, I calculated the average percentage difference between modeled and observed M2 amplitudes throughout

WY 2017. This error analysis confirmed that the model is indeed not representing Grizzly Bay accurately when compared to in-situ data, with percentage differences around 70%. Showing the percentage difference also highlights the decreased model skill of M2 amplitude replication in the Sacramento-San Joaquin Delta region. Down-estuary of the Carquinez Strait, the largest percentage difference is 4.8% at Redwood City. Upstream of the Carquinez Strait, the typical percentage difference in M2 amplitude is around 20%, with values as high as 54% in the southern region of the Delta.

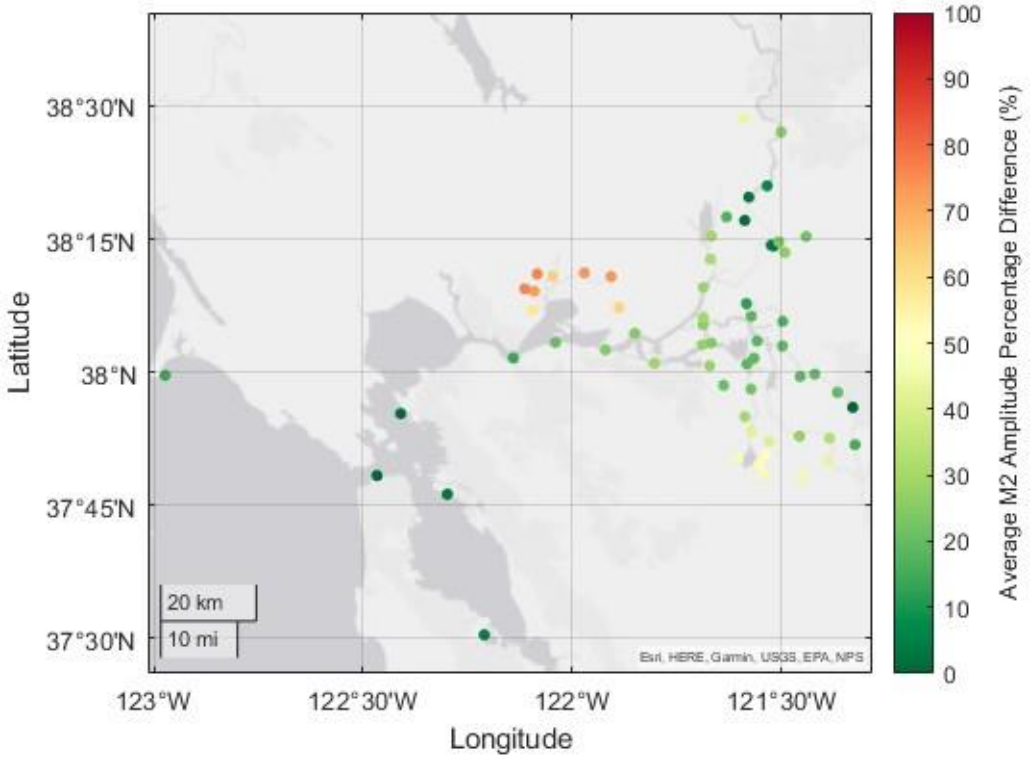

Figure 4.10: Average Percentage Error of M2 Amplitude for entirety of WY 2017 based on 332 trials of 32 day periods

4.1.3 WY2017 Riverine Impact on M2 Amplitude Model Performance

During WY2017, the M2 undergoes changes throughout the entire model domain. This is mostly due to river flow effects. The peak NDOI timing (Figure 4.3) correlates closely to both the observed and modeled minimum M2 values throughout the SFBD (Figure 4.1). At Alameda

(Figure 4.11), the modeled M2 decreases by 9.5% from the low flow period to the minimum M2 value. The observed M2 amplitude decreases by 12.5%. The timing for both minimum values is identical, but the model does not capture the full dampening effects caused by river flow.

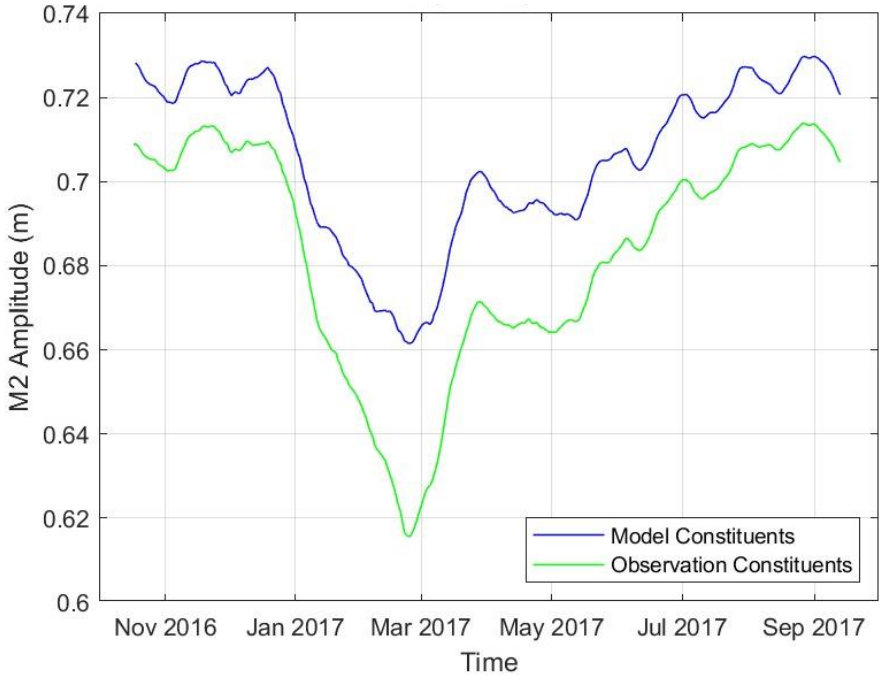

Figure 4.11: Modeled and observed M2 amplitudes at Alameda (NOAA Station 9414750) for WY2017

The observed M2 decreases on a range of 1.4% to 99.5%, with an average decrease of 41.1% (Figure 4.12). The modeled M2 decreases anywhere from 2.2-89.2% (average 42.0%) during the peak flow events of WY2017 (Figure 4.13). The modeled M2 is never fully diminished by river flow, even in the farthest-inland portions of the Sacramento-San Joaquin Delta, but the observed M2 shows an essentially fully diminished M2 amplitude near Sacramento at the riverside boundary of the model. The M2 amplitude is still influenced by low flow even during the high flow events because the length of the harmonic analysis input time series (32 days) is longer than the high-flow portion of the flood event (29 days over 6000 m^3/s). Thus, the 32 day period includes some periods of lower flow, with tidal motion. The modeled percent decrease results in the Grizzly Bay are unreliable due to the high RMSE of the results in that region.

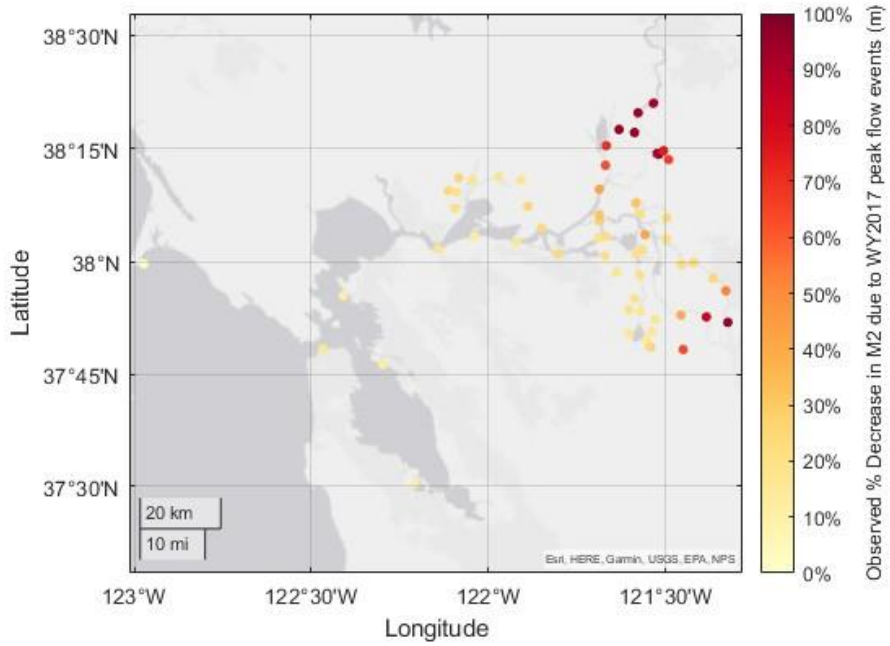

Figure 4.12: Observed Percent Decrease in M2 Amplitude due to Peak River Flow Effects of WY2017

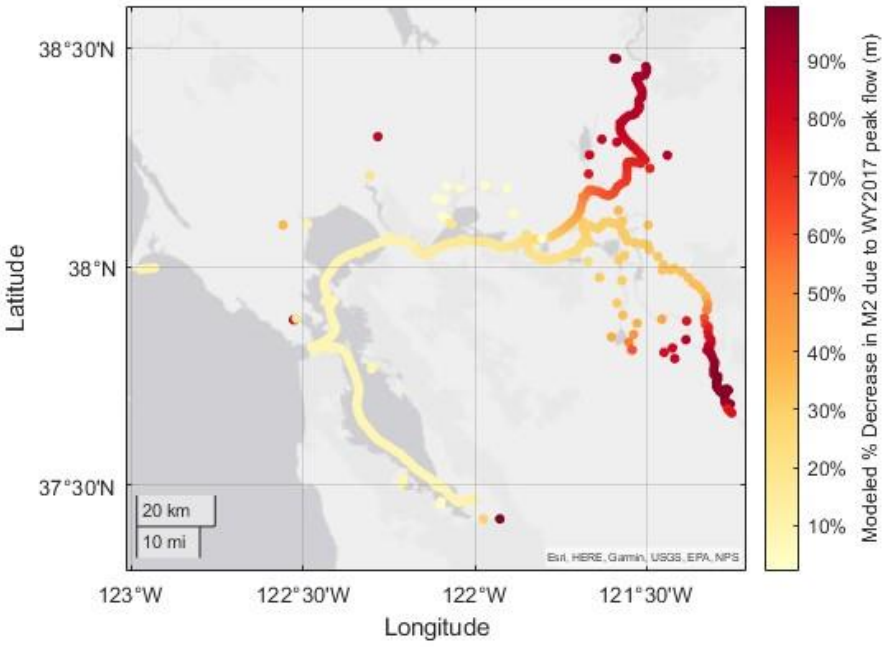

Figure 4.13: Modeled Percent Decrease in M2 Amplitude due to Peak River Flow Effects of WY2017

4.1.4 M2 Amplitude Model Performance versus Distance Upstream

The model observation points that form a line along the thalweg throughout the San Francisco Bay-Delta Region (Figure 4.14) were used to determine how the model represents the M2 as the distance from the ocean boundary increases. These points were placed approximately every 1 km and begin at the Golden Gate Bridge. The path follows the thalweg through the Central, San Pablo, and Suisun Bays then diverge to follow the separate thalwegs of the Sacramento River and San Joaquin River. It additionally follows the Southern thalweg into the South San Francisco Bay. The observation points terminate in the Delta region at the boundary of the model, and at the Southmost shoreline in the South San Francisco Bay.

Based on section 2.1.2, It was expected to see the overall decrease in M2 as distance upstream into the Delta increased. Additionally, the amplified tides in the South San Francisco Bay were captured by the model, as before noted in Holleman & Stacey (2014) [2]. This increase is seen by both the observed and modeled M2 amplitudes (Figure 4.15). The highest rate of M2 amplification occurs in the South Bay. Along the thalweg into the northern reach of the Central and San Pablo Bay, the largest M2 amplitude is seen at the 40 km mark, also similar to findings from previous studies [2]. The M2 begins to decrease upstream of the Carquinez Strait. These results are all consistent with the findings in Holleman & Stacey 2014. The spikes in M2 near Antioch (~Rkm 100) occur at the coupling between 1D and 2DH domains in the model and can be attributed to unrealistic tidal energy reflection at the linkage.

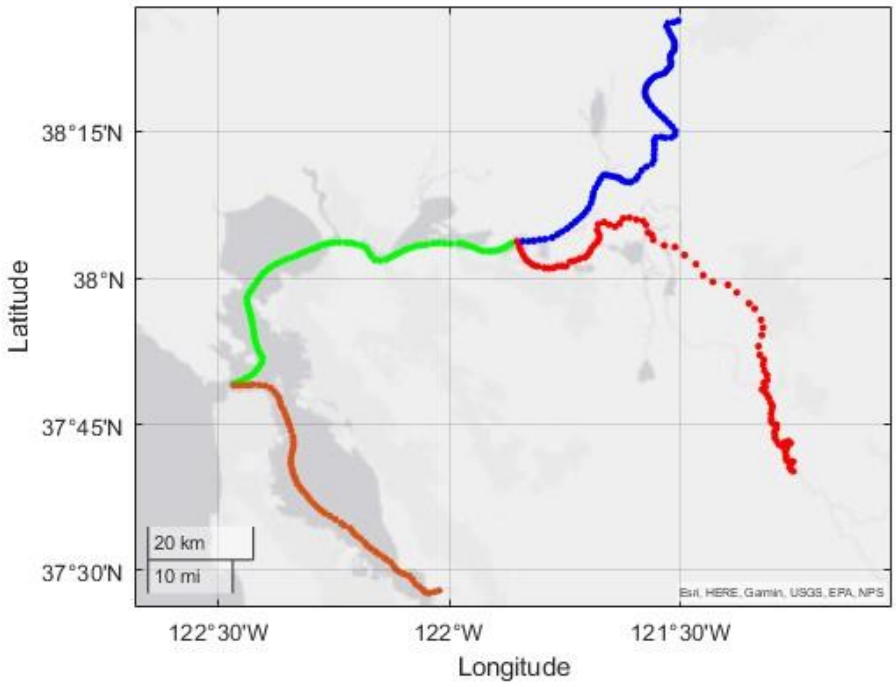

Figure 4.14: Path for Figure 4.12- Green represents the thalweg from the Golden Gate Bridge (GGB) to the 2DH boundary near Collinsville (0-100 Rkm), orange represents the thalweg from the GGB to the south end of the South Bay (0-75 Rkm), blue represents the thalweg

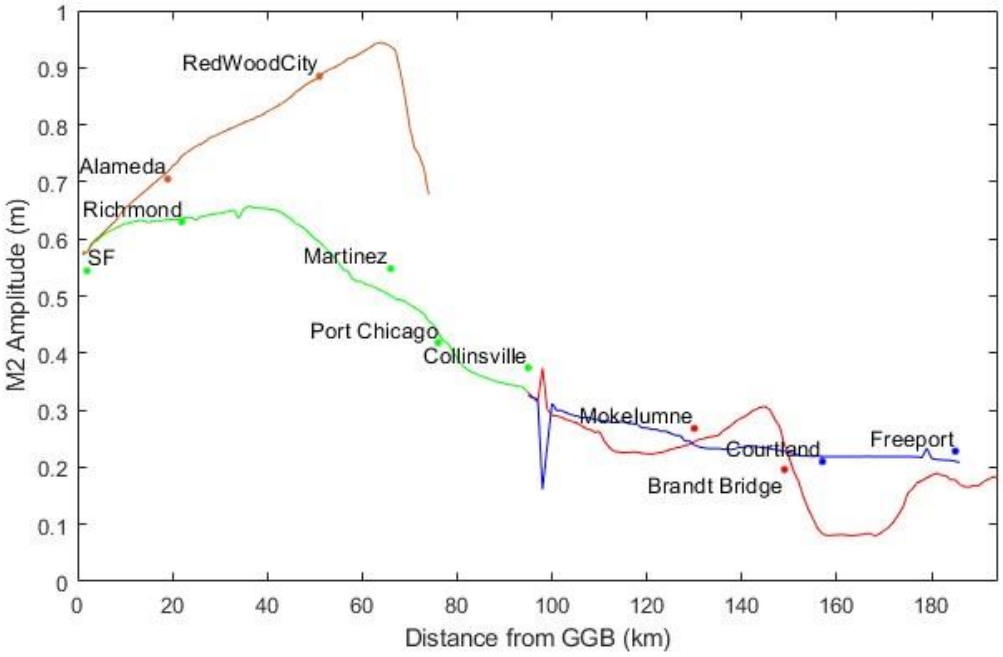

Figure 4.15: Low flow (November 1-December 3 2016) Modeled M2 tidal constituent along the thalweg from the GGB into San Francisco Bay (Green) into the Sacramento River (Blue), San Joaquin River (Red), and South Bay (Orange). Gauges along the thalweg are denoted with a dot and text.

The agreement between the modeled and observed M2 varies across the thalweg distance. The model performs within 6% error in the Central and South San Francisco Bay but begins to underestimate the M2 as the distance upstream increases past the Carquinez Strait (~45Rkm), with errors as high as 21.8% at Brandt Bridge on the Sacramento River. As the riverside boundary is approached in the Sacramento River, M2 skill increases again with error decreasing below 10%.

Table 4.2: Percent Difference of Modeled and Observed Values Displayed in Figure 4.12

Location	San Francisco	Alameda	Redwood City	Richmond	Martinez	Port Chicago	Collinsville	Mokelumne	Brandt Bridge	Courtland	Freeport
Modeled M2 Amplitude	0.5763	0.7176	0.8851	0.6356	0.5004	0.4368	0.3306	0.2443	0.2387	0.2187	0.2105
Observed M2 Amplitude	0.5444	0.705	0.885	0.6299	0.5479	0.418	0.3744	0.2681	0.1959	0.21	0.2281
% Difference	5.9	1.8	0.0	0.9	8.7	4.5	11.7	8.9	21.8	4.1	7.7

One possible reason for the overestimated decay in M2 amplitude upstream of the Carquinez Strait is that the cross-section is not conveying enough tidal flow, potentially due to insufficient grid resolution. The DEM utilized in the model was not the limiting factor, as the resolution was 10 m in this location, but the perpendicular grid resolution was roughly 50 m. Due to channel dredging, the depth increases rapidly perpendicular to flow at the Carquinez Strait. Because each grid utilizes the average depth for the cell, the modeled cross-sectional area may be smaller than reality, therefore constricting flow and decreasing the amount of tidal energy able to transmit upstream. Improvement effort results are discussed in section 4.2.4 and 4.2.5.

4.1.5 ERA5 Wind Forcing Accuracy

The ERA5 wind forcing utilized in the model from Nederhoff et al. 2021 provides hourly wind and air pressure values at 30 km resolution. When comparing the wind magnitude values from ERA5 to the nearest NOAA observation stations, misrepresentations of predominant wind direction was appreciably different (greater than 45^{o}) for 3 out of 7 NOAA stations analyzed. The ERA5 data underestimated wind magnitudes at 5 out of 7 gauges. For instance, both the wind magnitude and primary wind direction are different for the Richmond location (Figure 4.17). At Richmond, the primary wind direction is reported as westerly in the ERA5 reanalysis, but the NOAA meteorological station recorded the primary wind direction to be from the south-southeast. Overall, the ERA5 data overreports wind magnitudes from 1-4 m/s and underreports magnitudes over 5 m/s (Figure 4.16). Based on the wind sensitivity studies for both southerly and westerly winds, this suggests that better wind forcing might improve the skill with which water levels in summer and winter are modeled, particularly during periods of high storms.

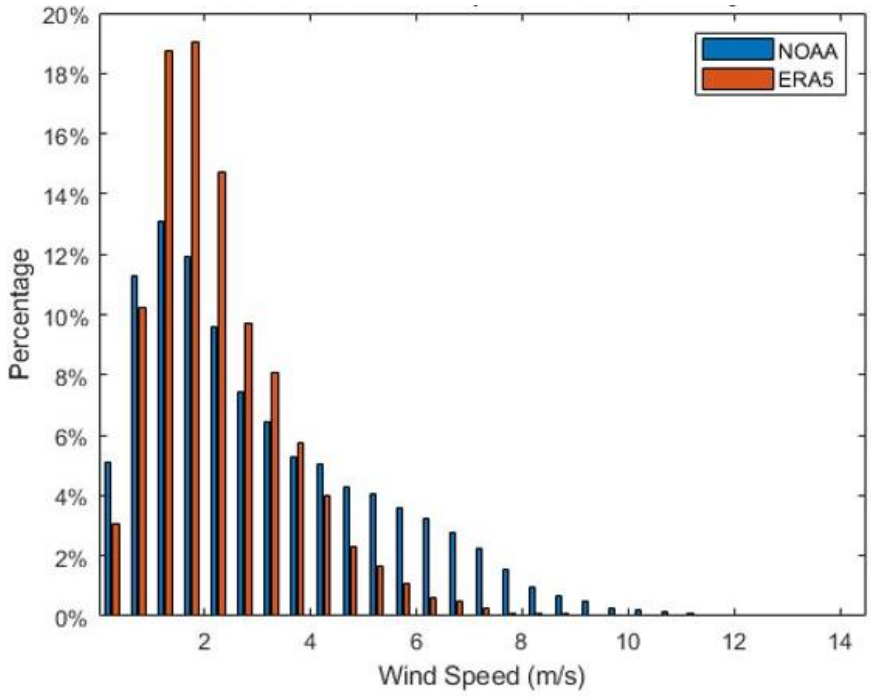

Figure 4.16: Probability Density Function of wind magnitude at NOAA Redwood City station 9414523 and the corresponding ERA5 grid datapoint

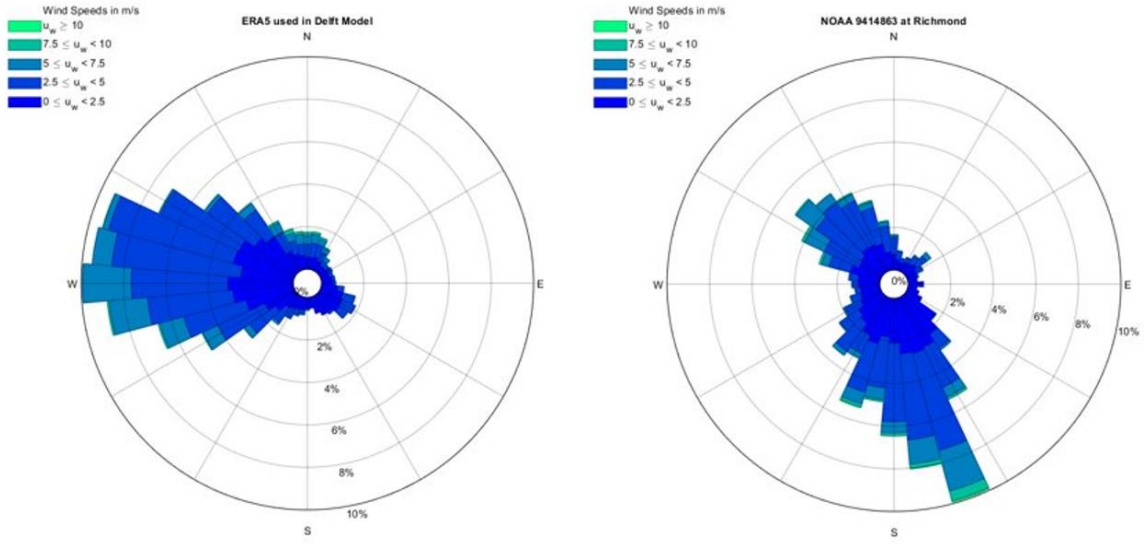

Figure 4.17: Wind roses representing the ERA5 wind forcing (left) and observed windspeeds for WY2017 at NOAA Richmond station 9414563

4.2 Experiments

This section details the results of the model experiments performed. The first section covers the effects of removing river flow on extreme water levels in the SFBD. The second section covers the results of the wind sensitivity study for two predominant wind directions in the SFBD.

4.2.1 River Flow Removal

This experiment aimed to identify the spatial and temporal effects of river flow on extreme water levels. One simulation run was conducted with only 300 m^3/s of river flow from the Sacramento River (WY17_Base), with zero flow from the smaller creeks that feed into the Bay. The second simulation (WY17_Full) was conducted with river flow simulating real conditions from WY2017. Both simulations were run from January 30th 2017 to March 14th 2017, in order to capture the major pluvial events of WY2017. Running the simulation for the same dates further isolates the river flow effects by maintaining the same oceanographic conditions.

The difference in the highest high water between these two runs (WY17_Base and WY17_Full) revealed how far downstream the high river flow affected extreme water levels. Self-evidently, the river flow had a major role in the extreme water levels at the Sacramento and San Joaquin River model boundaries (169 Rkm and 189 Rkm, respectively), elevating extreme water levels over 5.5 m (Figure 4.19). Once the Suisun Bay was reached, the riverine influence decreased, and west of the Carquinez Strait, the river flow had little impact on the extreme water levels (<0.05m) (Figures 4.18). Figures 4.18 and 4.19 are split into the Bay and Delta regions to better capture the gradients between the maximum and minimum values. The maximum value in Figure 4.18 is the minimum value in Figure 4.19. This indicates that in the South, Central, and San Pablo Bays, coastal storm surge and tidal processes are the main factors contributing to extreme water levels. M2 amplitude decreases throughout the bay and delta (Figure 4.12), but peak water elevations are still increased overall where riverine processes dominate flooding effects. This experiment showed very little increase in extreme water levels (highest high water levels) in the Bay (>0.05m) because the peak water levels occurred with the storm event. Much

later, river flows raised water levels by 0.16 m (Table 4.2), but this was less than the coastal storm surge.

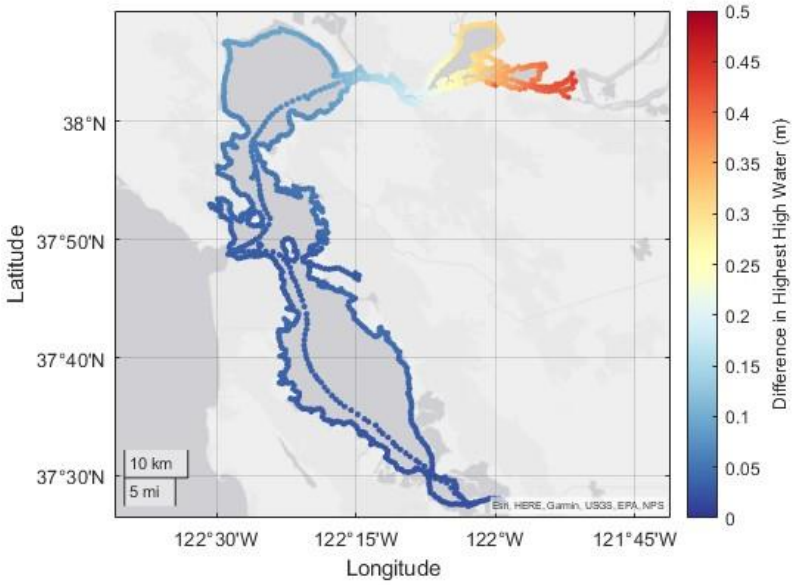

Figure 4.18: Difference in highest high waters between base and full conditions in the Bay Area (Note: axis from 0-0.5 m)

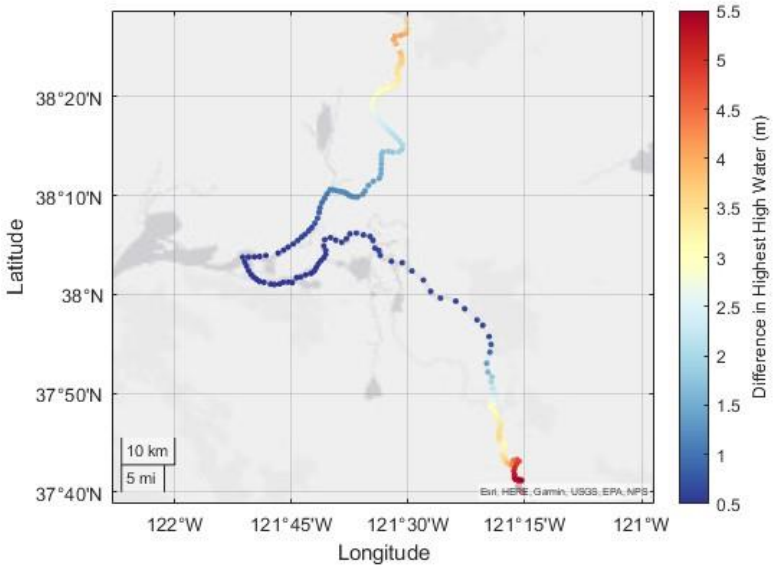

Figure 4.19: Difference in highest high waters between base and full conditions in the Delta (Note: axis from 0.5-5.5 m)

4.2.2 Wind Sensitivity Study- Southerly Wind

To understand the role of wind on extreme water levels in the San Francisco Bay and Delta regions, a uniform wind profile was applied for both westerly and southerly winds. Southerly winds are experienced during storm events when extreme water levels are likely to occur [62]. A constant southerly wind with various magnitudes from 0 to 20 m/s were applied for a 42 day period from January 30th, 2017, to March 14th, 2017, during the high river flow period. This sensitivity study showed that for the southerly winds, a constant wind does not start to notably affect water levels until the constant wind reaches a speed of 10 m/s. The gap in setup effects between 5 m/s and 10 m/s may be attributed to the square relationship between wind setup and wind speed in the Zuider Zee equation (Equation 6). For a wind speed of 10 m/s a setup is observed from the South Bay to the San Pablo, with decreased water levels by 0.09 m in the South Bay and increased water levels up to 0.08 m in the San Pablo Bay (Figure 4.20). For the largest southerly wind magnitude simulation, 20 m/s, water levels decreased up to 0.44 m in the South Bay and water levels in the San Pablo Bay increased by 0.40 m, reflecting previously noted setup/setdown symmetry [35]. It is also important to note that this constant wind for an extended duration of time is unrealistic, but this sensitivity study serves as a basis for the understanding the effect that wind setup has on water levels in this system.

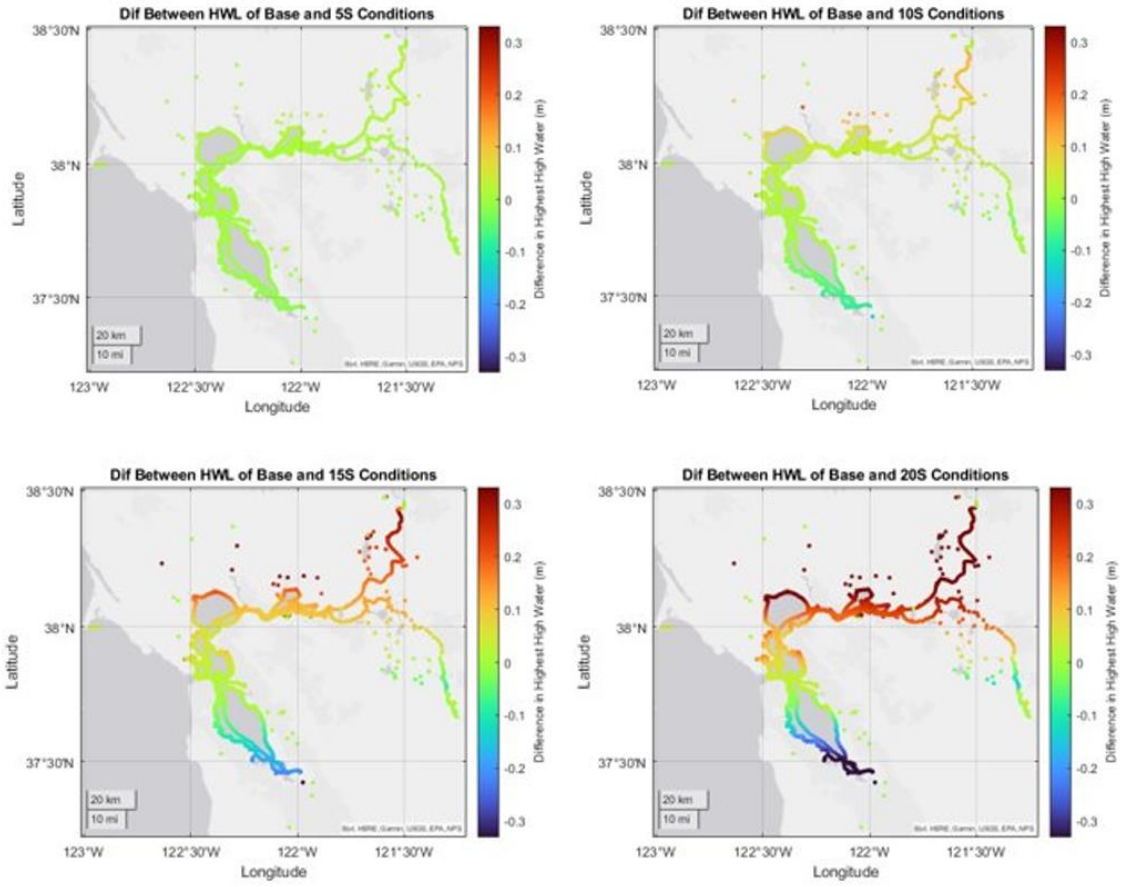

Figure 4.20: Highest High Water Level differences between 5, 10, 15, and 20 m/s constant southerly wind and base conditions (No wind, constant low flow from only the Sacramento River)

4.2.3 Wind Sensitivity Study- Westerly Wind

Westerly winds occur daily in the afternoon in the summer months [10], [47], [51], [57], [62]. For the westerly winds, a similar wind setup is seen starting at the 10 m/s simulation, and water levels in the entire San Francisco Delta region are especially elevated. In the 10 m/s simulation, water levels only slightly decreased in the windward direction by 0.02 m in the west end of the San Pablo Bay and increased water levels in the leeward direction of 0.22 m in the San Joaquin River. The South Bay water levels are also elevated by 0.09 m in the south-eastern corner of the bay. In the 20 m/s westerly wind simulations, water levels decreased in west San Pablo Bay by 0.15 m. Water levels in the Delta increased by 1.15 m and the southeastern corner

of the South Bay increased by 0.87 m, where the water collects with no path to flow elsewhere (Figure 4.21). The shorter fetch (compared to the N-S fetch of the South, Central, and San Pablo Bay) and constriction at the Carquinez Strait did not affect the intensity in which water levels were increased on the leeward side compared to the southerly wind experiment, however it may have caused the lack of setup/setdown symmetry observed in the southerly wind experiments and previous studies [35].

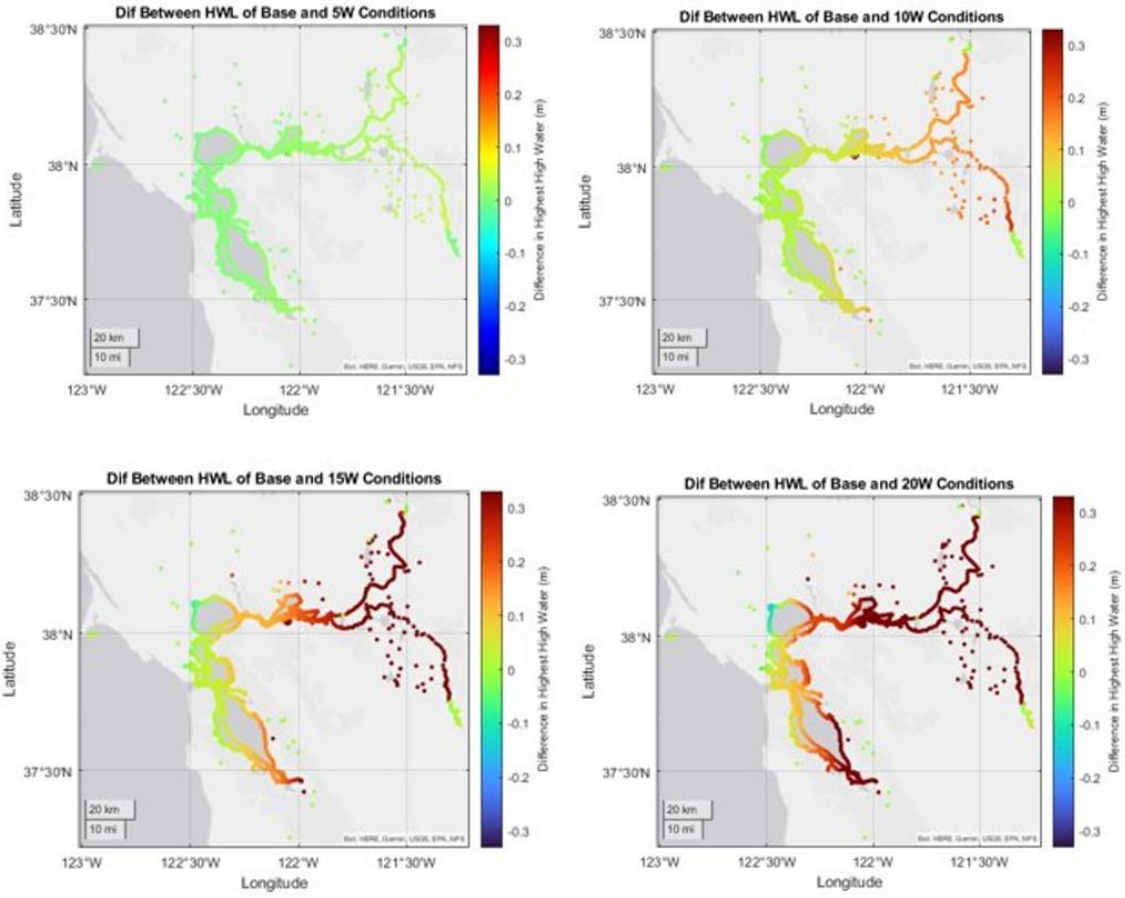

Figure 4.21: Highest High Water Level Differences between 5, 10, 15, and 20 m/s constant westerly wind and base conditions (No wind, constant low flow from only the Sacramento River)

4.2.4 Wind Forcing Improvement

Upon implementing a new wind forcing based on hourly data from 13 NOAA wind stations and airport wind gauges throughout the model domain, the wind forcing made very little

difference regarding both water level and M2 amplitude skill. The difference in M2 RMSE was on the scale of 0.0001 m. Since this change in forcing had minimal effects, I wanted to investigate the overall role that wind plays in water level and M2 skill. To do this, the model was run for the entire WY 2017 with a constant 0 m/s wind. During periods of high southerly winds, the area expected to see the most change is the long pitch that spans from the South Bay to the San Pablo Bay. The model captured the setup effects in this stretch of water. The South Bay timeseries shows that the model, when ran with the ERA5 wind forcing, experienced a decreased peak and trough water levels (>0.1m) (Figure 4.22). Meanwhile, the San Pablo Bay experienced elevated peak and trough water levels (>0.1m) (Figure 4.23).

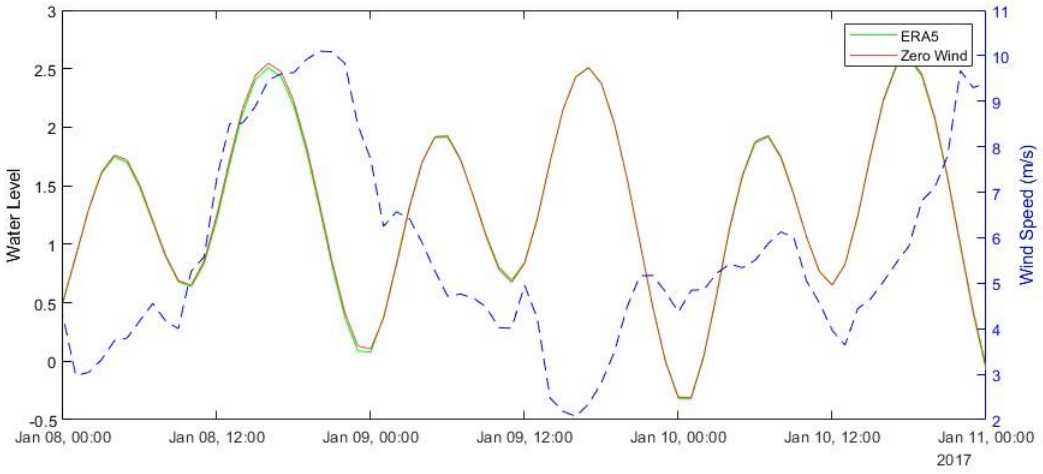

Figure 4.22: South Bay water level time series during high wind period; Green represents the water level timeseries (m) using the same wind forcing from Nederhoff et al. (2021), red represents the water levels of a simulation with a constant 0 m/s wind for the entirety of the year (m), and blue represents the ERA5 wind magnitude (m/s)

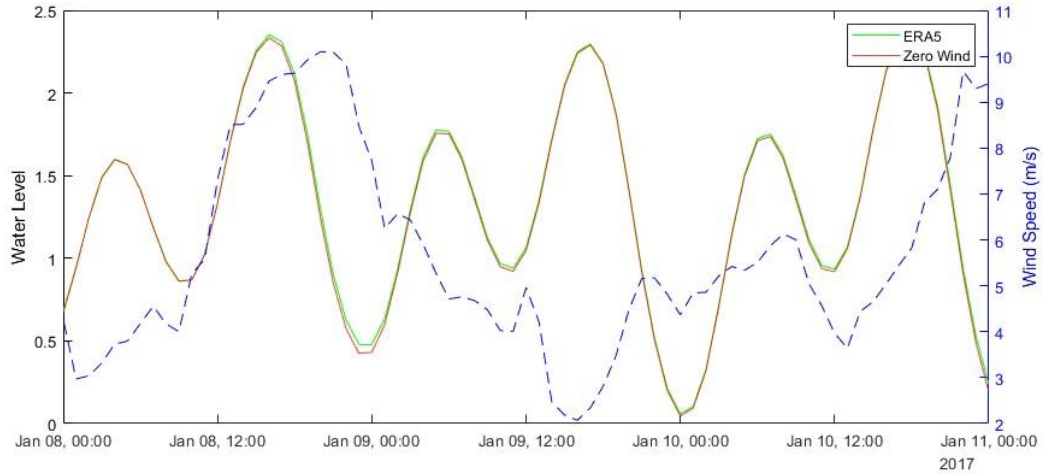

Figure 4.23: San Pablo Bay (north of South Bay) time series during high wind period with the same representations as Figure 4.20

The mean water level was affected by around 0.03 m at most in a comparison of the zero wind (WY17_Base) and ERA5 wind (WY17_Full) simulations during low flow periods (Figure 4.24). For most of the stations, the ERA5 wind forcing model performed better than the zero wind

model, but none of these improvements brought the water levels drastically closer to observed conditions.

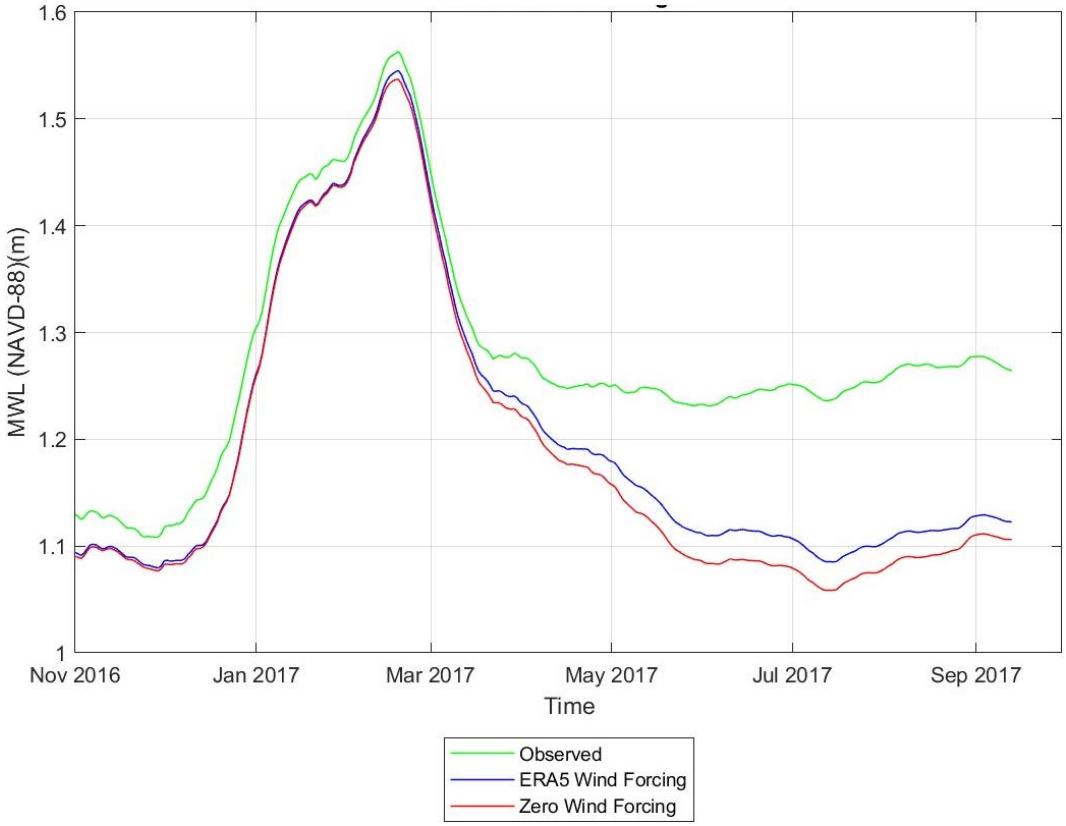

Figure 4.24: Observed, ERA5 wind forcing, and zero wind forcing 32-day MWLs for WY 2017 at Port Chicago

The M2 amplitude was also affected by the removal of a wind forcing. The M2 amplitude either increased or decreased by 0.005 m at most and the M2 amplitude RMSE was increased by 0.002 m at most (Figure 4.25). The effects on the M2 amplitude of the zero wind forcing varied throughout the model. The M2 amplitude decreased in some regions but also increased in other areas such as Port Chicago (Figure 4.25). This varying difference in M2 therefore did not correlate to a steady improvement or decline in RMSE. Still, no previous analysis to my knowledge has linked wind forcing and the additional mixing and currents it produces to altered tidal properties. This study shows that wind exerts a small, but not negligible, effect on the M2 tide (~1%). However, we did not include the effects of waves or ocean swell, which can be important in estuaries, especially at estuary inlets [64].

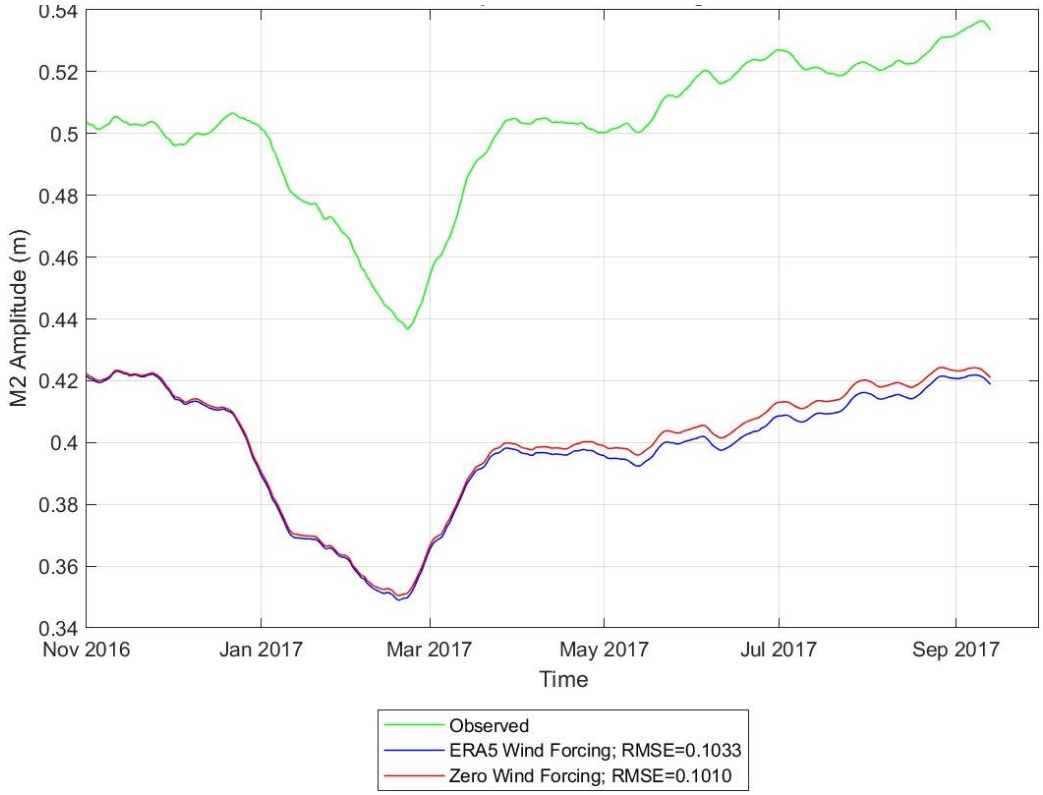

Figure 4.25: Observed, ERA5 wind forcing, and zero wind forcing M2 amplitudes spanning WY 2017 at Port Chicago with RMSE statistics

4.2.5 Model Grid Refinement

I doubled the number of cells that span the 800 m wide cross section at the Carquinez Strait (Figure 3.6). This improved the cross-river resolution to 25 m. I kept the orthogonality of the improved grid low enough to initialize the model and simulate the entire WY2017 without crashing. The original peak orthogonality value was 0.130. After modifications it was 0.257. This value was low enough to run the model for the entire WY2017 without crashing. However, the modifications of the grid broke the coupling between 1D and 2DH domains which caused reflection effects and completely restricted fluvial flow from the 1D domain. The coupling of the 1D-2D model was a customized, non-standard model attribute, and I was unable to fix the issue.

Chapter 5

CONCLUSION

5.1 Summary of Results

The 1D/2DH model of the San Francisco Bay and Sacramento-San Joaquin Delta outlined in Nederhoff et al (2021) was evaluated on multiple metrics of performance through the WY2017, a year marked by substantial river discharge during the winter. This model was developed from the 2D model from Martyr-Koller et al (2017). A total of 70 gauges were used to assess the model skill throughout San Francisco Bay and Delta region. Additionally, boundary conditions in 10 experimental model simulations were changed to evaluate the influence of river flow and wind forcing. Attempts to improve the model through increased grid resolution and a more accurate wind forcing were unsuccessful.

The Delft3D Flow FM 1D/2DH model (Nederhoff et al 2021) was evaluated on the ability to replicate water levels and the M2 amplitude. The average M2 amplitude RMSE among all observed stations in the model domain was 0.089 m (N = 332). The model struggled most replicating the tidal range in Grizzly Bay, just west of the Delta and east of the Carquinez Strait (RMSE ~0.5 m). The poor validation is likely due to the complex and shallow bathymetry of this estuarine marsh. The Delta region often underrepresented both water levels and M2 amplitudes, likely due to over-restricted upstream water confluence at the Carquinez Strait. Qualitatively, the model captured the inverse relationship between river flow and the M2 amplitude throughout the entire year at a vast majority of the observed stations and thus was deemed appropriate for use investigating how riverine, oceanic, and atmospheric processes influence high water levels throughout this complex system.

The 2D modeling approach may underestimate river-tide interactions in the bottom stress term, and/or baroclinic and stratification effects play a larger role in tidal damping than previously assumed. Because modeled M2 amplitudes are estimated to be damped during the peak of the Feb. 2017 discharge event, the underestimation in M2 may impact modeled flood waters.

Model trials with near-zero river flow (300 m^3/s) highlighted the regions that are affected by river flow when compared to the trial with realistic forcing. Riverine forcing had an impact on extreme water levels from the eastern boundary of the model in both the Sacramento and San Joaquin Rivers (~185 Rkm from the GGB) to the Carquinez Strait (~45 Rkm from the GGB), seeing elevated water levels up to 2m, with typical increases closer to 0.5m. At the highest water level, NDO was ~11,000 m^3/s. In the San Pablo, Central, and South Bay, the highest water level decreased less than 0.10 m when river flow was removed.

The influence of wind forcing on high water levels was explored by applying constant wind speeds, consistent with storm and summertime wind patterns, respectively. The influence of a constant 5 m/s wind was minor and raised water levels less than 0.05 m regardless of wind direction. The 10 to 20 m/s southerly simulations produced a more substantial influence. Elevated water levels increased by 0.40 m in the largest magnitude southerly wind scenario (20 m/s) in the San Pablo Bay, Suisun Bay, and northern reach of the modeled Sacramento River. Water levels decreased up to 0.44 m in the South Bay, reflecting previously noted setup/setdown symmetry [35]. In the 20 m/s westerly wind simulations, water levels only slightly decreased on the windward side of the model in west San Pablo Bay (0.15 m) when compared to the increased water levels in the Delta (1.15 m) and the southeastern corner of the South Bay (0.87 m). These setdown/setup values do not reflect the symmetry produced in the southerly wind experiments and previous studies [35]. The constant wind forcing is unlikely to persist for days and so the modeled results are likely an overprediction. Nonetheless, the sensitivity study provides insights into the pattern of wind setup and setdown that might happen over steady state conditions. The simulations suggest that the southerly wind that typically precedes extratropical storms in the Bay Area is likely a small, but not negligible contributor to high water levels and flood risk in the Northern San Francisco Bay region. Also, at the same time, extreme water levels in the South Bay may be somewhat diminished. However, the possible effect of basin-scale seiching after wind diminishes was not explored. The effects of wind-induced waves and above water topography were not considered.

Wind forcing and the enhanced circulation and mixing it produces has a small effect on the modulation of the M2 amplitude (though waves are not considered). The difference between the two simulations revealed that the M2 amplitude was affected by 0.005 m at most, at Port Chicago, a ~1% shift. The wind effects on the modeled M2 amplitude were not consistent; the wind sometimes increased and sometimes decreased the M2 amplitude. The wind forcing effect was also not consistent on error, however this was very marginal, only altering the M2 amplitude RMSE by 0.002 m (1.2%) at most.

5.2 Recommendations for Improvements and Future Analysis

This thesis has shown how river flow influences the San Francisco Bay, both directly by raising tidally averaged water levels, but also indirectly by decreasing M2, even in regions not directly influenced by river flow currents (like the South San Francisco Bay region). Wind stress also acts to increase and decrease water levels and can produce slight (~1%) changes to the M2 tide. The influence of these non-linear wind-river-tide interactions on extremes depends on their timing, relative to when the peak occurs. For example, when coastal processes (such as tides and storm surge) dominate the peak water level, the river-tide interaction is not consequential, since it occurs much later. Therefore, more work needs to be done to evaluate the influence of event timing on changes to water levels. The reasons for M2 changes and why they do not completely match measurements needs to be investigated. For example, it is possible that 3D effects such as stratification play a role.

Attempts to improve the model were not successful in the amount of time available. Improvements through increasing the grid resolution while maintaining proper linkage between the 1D network and 2DH grid required software that, at the time of publishing, is unavailable to the public. A more fundamental solution, developing a 2D model grid for the Delta, was beyond the scope of the project. Increasing the grid resolution successfully at the Carquinez Strait could allow for more accurate representation of upstream tidal amplitudes and improve the fidelity of fluvial/tidal interactions. Hydrodynamic effects of channel dredging, shoreline modification (seawalls), and wetland restoration could then be further explored utilizing this model.

Increasing the spatial resolution of the wind forcing in the model could lead to better results. The ERA5 forcing utilized is a medium-range reanalysis with a 30km resolution. A finer resolution wind model would help account for the mountainous terrain in the Bay area, increasing the accuracy of representative wind directions and magnitudes.

The wind sensitivity study could be expanded upon. Only 4 magnitudes and 2 directions were examined. In Gurumurthy et al (2019), 16 wind directions were analyzed in a similar experiment. Additionally, the gap in response between the 5 m/s and 10 m/s trials in this experiment is large, especially considering that wind setup and wind velocity have a square relationship (see Equation 6). Running simulations in between these magnitudes could reveal if the windspeed-wind setup response in the San Francisco Bay follows this square relationship (Equation 6) [34].

Investigation into small and medium tributary flows in the Bay Area could be examined. Specifically, how the time scales of storms may interact differently with the shorter response time of tributary flow when compared to Delta inflow. Since the time of concentration would be shorter for these smaller rivers, it is more likely for river flow and storm surge to interact and form a compound event.

This research only covered one high flow year, whereas the model it is evaluating simulated 69 years. More analysis during high flow years can lead to a better understanding of river effects on the hydrodynamics in the San Francisco Bay. WY2023 will be an interesting year to analyze once the data is available, as it is marked by large rainfall events and flooding throughout California.

REFERENCES

[1] K. R. Dyer, “Estuaries; A Physical Introduction,” 1973.

[2] R. C. Holleman and M. T. Stacey, “Coupling of sea level rise, tidal amplification, and inundation,” *J Phys Oceanogr*, vol. 44, no. 5, pp. 1439–1455, 2014, doi: 10.1175/JPO-D-13-0214.1.

[3] E. Szlemp, “ANALYSIS OF THE TIDAL RANGE IN THE SACRAMENTO SAN JOAQUIN DELTA FROM 1857 TO PRESENT,” 2020.

[4] H. R. Moftakhari, D. A. Jay, S. A. Talke, T. Kukulka, and P. D. Bromirski, “A novel approach to flow estimation in tidal rivers,” *Water Resour Res*, vol. 49, no. 8, pp. 4817–4832, Aug. 2013, doi: 10.1002/wrcr.20363.

[5] “State of California The Natural Resources Agency DEPARTMENT OF WATER RESOURCES Bay-Delta Office,” 2016.

[6] F. Bay *et al.*, “Hydrodynamic and Water Quality Model Calibration and Application in San.”

[7] R. C. Martyr-Koller *et al.*, “Application of an unstructured 3D finite volume numerical model to flows and salinity dynamics in the San Francisco Bay-Delta,” *Estuar Coast Shelf Sci*, vol. 192, pp. 86–107, Jun. 2017, doi: 10.1016/j.ecss.2017.04.024.

[8] D. Pugh, *Tides, surges, and mean sea-level*. J. Wiley, 1987.

[9] “Basic Information About Estuaries,” Environmental Protection Agency. Accessed: Nov. 27, 2023. [Online]. Available: https://19january2017snapshot.epa.gov/nep/basic-information-about-estuaries_.html

[10] W. J. Kimmerer, “Open Water Processes of the San Francisco Estuary: From Physical Forcing to Biological Responses,” *San Francisco Estuary and Watershed Science*, vol. 2, no. 1, Feb. 2004, doi: 10.15447/sfews.2004v2iss1art1.

[11] J. Wang, H. E. de Swart, and Y. M. Dijkstra, “Dependence of tides and river water transport in an estuarine network on river discharge, tidal forcing, geometry and sea level rise,” *Cont Shelf Res*, vol. 225, Aug. 2021, doi: 10.1016/j.csr.2021.104476.

[12] D. A. Jay, “Green’s law revisited: Tidal long-wave propagation in channels with strong topography,” *J Geophys Res Oceans*, vol. 96, no. C11, pp. 20585–20598, Nov. 1991, doi: 10.1029/91jc01633.

[13] G. Godin, “The Propagation of Tides up Rivers With Special Considerations on the Upper Saint Lawrence River,” 1999. [Online]. Available: http://www.idealibrary.comon

[14] C. T. Friedrichs and D. G. Aubrey, “Tidal propagation in strongly convergent channels,” *J Geophys Res*, vol. 99, no. C2, pp. 3321–3336, 1994, doi: 10.1029/93JC03219.

[15] S. Lanzoni and G. Seminara, “On tide propagation in convergent estuaries,” *J Geophys Res Oceans*, vol. 103, no. C13, pp. 30793–30812, Dec. 1998, doi: 10.1029/1998jc900015.

[16] L. C. Van Rijn, “Analytical and numerical analysis of tides and salinities in estuaries; Part I: Tidal wave propagation in convergent estuaries,” in *Ocean Dynamics*, Nov. 2011, pp. 1719–1741. doi: 10.1007/s10236-011-0453-0.

[17] S. A. Talke and D. A. Jay, “Changing Tides: The Role of Natural and Anthropogenic Factors,” 2020, doi: 10.1146/annurev-marine-010419.

[18] N. J. Nidzieko, “Tidal asymmetry in estuaries with mixed semidiurnal/diurnal tides,” *J Geophys Res Oceans*, vol. 115, no. 8, 2010, doi: 10.1029/2009JC005864.

[19] B. Lieberthal, K. Huguenard, L. Ross, and K. Bears, “The Generation of Overtides in Flow Around a Headland in a Low Inflow Estuary,” *J Geophys Res Oceans*, vol. 124, no. 2, pp. 955–980, Feb. 2019, doi: 10.1029/2018JC014039.

[20] S. A. Talke and M. T. Stacey, “Suspended sediment fluxes at an intertidal flat: The shifting influence of wave, wind, tidal, and freshwater forcing,” *Cont Shelf Res*, vol. 28, no. 6, pp. 710–725, Apr. 2008, doi: 10.1016/j.csr.2007.12.003.

[21] A. S. Chernetsky, H. M. Schuttelaars, and S. A. Talke, “The effect of tidal asymmetry and temporal settling lag on sediment trapping in tidal estuaries,” *Ocean Dyn*, vol. 60, no. 5, pp. 1219–1241, Oct. 2010, doi: 10.1007/s10236-010-0329-8.

[22] B. B. Parker, C. M. Gutierrez, C. C. Lautenbacher, J. H. Dunnigan, A. Administrator, and M. Szabados, “Tidal Analysis and Prediction Center for Operational Oceanographic Products and Services,” 2007. [Online]. Available: http://tidesandcurrents.noaa.gov

[23] H. Cai, H. H. G. Savenije, and M. Toffolon, “Linking the river to the estuary: Influence of river discharge on tidal damping,” *Hydrol Earth Syst Sci*, vol. 18, no. 1, pp. 287–304, Jan. 2014, doi: 10.5194/hess-18-287-2014.

[24] S. Vongvisessomjai and S. Rojanakamthorn, “INTERACTION OF TIDE AND RIVER FLOW.”

[25] J. J. Dronkers, *Tidal computations in rivers and coastal waters.* Amsterdam: North-Holland Pub. Co., 1964.

[26] A. C. Horrevoets, H. H. G. Savenije, J. N. Schuurman, and S. Graas, “The influence of river discharge on tidal damping in alluvial estuaries,” *J Hydrol (Amst)*, vol. 294, no. 4, pp. 213–228, Jul. 2004, doi: 10.1016/j.jhydrol.2004.02.012.

[27] S. A. Talke, R. Familkhalili, and D. A. Jay, “The Influence of Channel Deepening on Tides, River Discharge Effects, and Storm Surge,” *J Geophys Res Oceans*, vol. 126, no. 5, May 2021, doi: 10.1029/2020JC016328.

[28] D. K. Ralston, S. Talke, W. R. Geyer, H. A. M. Al-Zubaidi, and C. K. Sommerfield, “Bigger Tides, Less Flooding: Effects of Dredging on Barotropic Dynamics in a Highly Modified Estuary,” *J Geophys Res Oceans*, vol. 124, no. 1, pp. 196–211, Jan. 2019, doi: 10.1029/2018JC014313.

[29] “Normal Depth Demonstration Tool,” National Weather Service. Accessed: Nov. 27, 2023. [Online]. Available: https://www.weather.gov/aprfc/NormalDepthCalc

[30] S. G. Monismith, J. R. Burau, and M. T. Stacey, “Structure and Flow-Induced Variability of the Subtidal Salinity Field in Northern San Francisco Bay,” 2002.

[31] B. S. Giese, D. A. Jay, and G. Program, “Modelling Tidal Energetics of the Columbia River Estuary,” 1989.

[32] A. J. H. Simpson, “A simple model of estuarine subtidal fluctuations forced by local and remote wind stress,” *J Geophys Res Oceans*, vol. 90, no. C6, pp. 11945–11948, Nov. 1985, doi: 10.1029/jc090ic06p11945.

[33] D. A. Jay and J. D. Musiak, “Particle trapping in estuarine tidal flows,” *J Geophys Res*, vol. 99, no. C10, 1994, doi: 10.1029/94jc00971.

[34] G. Loiselle *et al.*, “A semi-empirical wind set-up forecasting model for Lake Champlain,” *Hydrol Process*, vol. 35, no. 6, Jun. 2021, doi: 10.1002/hyp.14240.

[35] P. Gurumurthy, P. M. Orton, S. A. Talke, N. Georgas, and J. F. Booth, “Mechanics and historical evolution of sea level blowouts in New York harbor,” *J Mar Sci Eng*, vol. 7, no. 5, May 2019, doi: 10.3390/jmse7050160.

[36] F. J. Rueda and S. G. Schladow, “Surface seiches in lakes of complex geometry,” *Limnol Oceanogr*, vol. 47, no. 3, pp. 906–910, 2002, doi: 10.4319/lo.2002.47.3.0906.

[37] C. Li, W. Huang, C. Chen, and H. Lin, “Flow Regimes and Adjustment to Wind-Driven Motions in Lake Pontchartrain Estuary: A Modeling Experiment Using FVCOM,” *J Geophys Res Oceans*, vol. 123, no. 11, pp. 8460–8488, Nov. 2018, doi: 10.1029/2018JC013985.

[38] J. Zscheischler *et al.*, “Future climate risk from compound events,” *Nature Climate Change*, vol. 8, no. 6. Nature Publishing Group, pp. 469–477, Jun. 01, 2018. doi: 10.1038/s41558-018-0156-3.

[39] S. L. Dykstra, B. Dzwonkowski, and R. Torres, “The Role of River Discharge and Geometric Structure on Diurnal Tidal Dynamics, Alabama, USA,” *J Geophys Res Oceans*, vol. 127, no. 3, Mar. 2022, doi: 10.1029/2021JC018007.

[40] H. Moftakhari, J. E. Schubert, A. AghaKouchak, R. A. Matthew, and B. F. Sanders, “Linking statistical and hydrodynamic modeling for compound flood hazard assessment in tidal channels and estuaries,” *Adv Water Resour*, vol. 128, pp. 28–38, Jun. 2019, doi: 10.1016/j.advwatres.2019.04.009.

[41] L. T. Helaire, S. A. Talke, D. A. Jay, and H. Chang, “Present and Future Flood Hazard in the Lower Columbia River Estuary: Changing Flood Hazards in the Portland-Vancouver Metropolitan Area,” *J Geophys Res Oceans*, vol. 125, no. 7, Jul. 2020, doi: 10.1029/2019JC015928.

[42] S. Mukhopadhyay, M. Leung, L. Cagigal, J. Kucharski, P. Ruggiero, and S. Steinschneider, “Understanding the Natural Variability of Still Water Levels in the San Francisco Bay Over the Past 500 yr: Implications for Future Coastal Flood Risk,” *J Geophys Res Oceans*, vol. 128, no. 2, Feb. 2023, doi: 10.1029/2022JC019012.

[43] M. Peng, R. A. Schmalz, A. Zhang, and F. Aikman, “Towards the development of the National Ocean Service San Francisco bay Operational forecast system,” *J Mar Sci Eng*, vol. 2, no. 1, pp. 247–286, Mar. 2014, doi: 10.3390/jmse2010247.

[44] R. Pawlowicz, B. Beardsley, and S. Lentz, “Classical tidal harmonic analysis including error estimates in MATLAB using T TIDE $,” 2002. [Online]. Available: http://www.ocgy.ubc.ca/~rich.

[45] “Harmonic Analysis,” NOAA. Accessed: Nov. 27, 2023. [Online]. Available: https://tidesandcurrents.noaa.gov/harmonic.html#:~:text=The%20mathematical%20process%20by%20which,separated%20into%20basic%20harmonic%20constituents

[46] D. L. Codiga, “Unified tidal analysis and prediction using the UTide Matlab functions,” 2011, doi: 10.13140/RG.2.1.3761.2008.

[47] T. J. Conomos, R. E. Smith, and J. W. Gartner, “Environmental setting of San Francisco Bay.”

[48] M. A. Hummel and M. T. Stacey, “Assessing the Influence of Shoreline Adaptation on Tidal Hydrodynamics: The Role of Shoreline Typologies,” *J Geophys Res Oceans*, vol. 126, no. 2, Feb. 2020, doi: 10.1029/2020JC016705.

[49] S. A. Talke and D. A. Jay, “Nineteenth century north american and pacific tidal data: Lost or just forgotten,” *J Coast Res*, vol. 29, no. 6 A, pp. 118–127, Nov. 2013, doi: 10.2112/JCOASTRES-D-12-00181.1.

[50] “Map showing channel width of Carquinez Strait at Frank Zappa Memorial Bridge,” Google Earth. Accessed: Oct. 19, 2023. [Online]. Available: earth.google.com/web/

[51] P. L. Barnard, D. H. Schoellhamer, B. E. Jaffe, and L. J. McKee, “Sediment transport in the San Francisco Bay Coastal System: An overview,” *Mar Geol*, vol. 345, pp. 3–17, Nov. 2013, doi: 10.1016/j.margeo.2013.04.005.

[52] H. R. Moftakhari, D. A. Jay, S. A. Talke, and D. H. Schoellhamer, “Estimation of historic flows and sediment loads to San Francisco Bay, 1849-2011,” *J Hydrol (Amst)*, vol. 529, pp. 1247–1261, Oct. 2015, doi: 10.1016/j.jhydrol.2015.08.043.

[53] L. P. Disney, “Tides and Currents in San Francisco Bay”.

[54] M. D. Marineau and S. A. Wright, “Effects of human alterations on the hydrodynamics and sediment transport in the Sacramento-San Joaquin Delta, California,” in *IAHS-AISH Proceedings and Reports*, Copernicus GmbH, 2014, pp. 399–406. doi: 10.5194/piahs-367-399-2015.

[55] J. E. Cloern *et al.*, “Projected evolution of California’s San Francisco bay-delta-river system in a century of climate change,” *PLoS One*, vol. 6, no. 9, Sep. 2011, doi: 10.1371/journal.pone.0024465.

[56] N. Knowles, “Natural and management influences on freshwater inflows and salinity in the San Francisco Estuary at monthly to interannual scales,” *Water Resour Res*, vol. 38, no. 12, pp. 25-1-25–11, Dec. 2002, doi: 10.1029/2001wr000360.

[57] H. Baranes, S. A. Talke, D. Jay, and S. L. Dykstra, “Sea level rise and the drivers of daily water levels in the.”

[58] A. R. Enríquez *et al.*, “Predictable Changes in Extreme Sea Levels and Coastal Flood Risk Due To Long-Term Tidal Cycles,” *J Geophys Res Oceans*, vol. 127, no. 4, Apr. 2022, doi: 10.1029/2021JC018157.

[59] M. Shirzaei and R. Bürgmann, “Global climate change and local land subsidence exacerbate inundation risk to the San Francisco Bay Area,” 2018. [Online]. Available: https://www.science.org

[60] California Department of Water Resources, “Dayflow,” 2019. Accessed: Nov. 07, 2023. [Online]. Available: https://data.ca.gov/dataset/dayflow

[61] “Prevailing Wind Direction,” Western Regional Climate Center. Accessed: Oct. 31, 2023. [Online]. Available: https://wrcc.dri.edu/Climate/comp_table_show.php?stype=wind_dir_avg

[62] S. G. T. Pubben, “3D MIXING PATTERNS IN SAN FRANCISCO SOUTH BAY,” 2017.

[63] G. Griggs *et al.*, “Rising Seas in California - An Update on Sea Level Rise Science.”

[64] S. A. Talke and M. T. Stacey, “The influence of oceanic swell on flows over an estuarine intertidal mudflat in San Francisco Bay,” *Estuar Coast Shelf Sci*, vol. 58, no. 3, pp. 541–554, 2003, doi: 10.1016/S0272-7714(03)00132-X.

[65] “Biological Opinion on Long-term Operation of the Central Valley Project and the State Water Project,” 2019. doi: 10.25923/f6tw-rkl.

[66] S. Monismith and J. R. Burau, “Stratification Dynamics and Gravitational Circulation in Northern San Francisco Bay,” 1996.

[67] Z. Wang *et al.*, “Light Regulation of Phytoplankton Growth in San Francisco Bay Studied Using a 3D Sediment Transport Model,” *Front Mar Sci*, vol. 8, Jun. 2021, doi: 10.3389/fmars.2021.633707.

[68] K. Nederhoff *et al.*, “Drivers of extreme water levels in a large, urban, high-energy coastal estuary – A case study of the San Francisco Bay,” *Coastal Engineering*, vol. 170, Dec. 2021, doi: 10.1016/j.coastaleng.2021.103984.

[69] “Delft3D 3D/2D User Manual.”

[70] “National Water Information System: Web Interface,” USGS. Accessed: Nov. 27, 2023. [Online]. Available: https://waterdata.usgs.gov/ca/nwis/current/?type=flow

[71] J. J. Danielson *et al.*, “Topobathymetric elevation model development using a new methodology: Coastal national elevation database,” *J Coast Res*, vol. 76, no. sp1, pp. 75–89, Dec. 2016, doi: 10.2112/SI76-008.

[72] Fregoso and Theresa, “A New Seamless, High-Resolution Digital Elevation Model of the San Francisco Bay-Delta Estuary, California”.

[73] H. Hersbach *et al.*, “The ERA5 global reanalysis,” *Quarterly Journal of the Royal Meteorological Society*, vol. 146, no. 730, pp. 1999–2049, Jul. 2020, doi: 10.1002/qj.3803.

[74] “LLJP Wind Shear Formula (Power law),” NOAA.

[75] “Hydroclimate Report,” 2017.

[76] R. A. Branch, A. R. Horner-Devine, C. C. Chickadel, S. A. Talke, D. Clark, and A. T. Jessup, “Surface Turbulence Reveals Riverbed Drag Coefficient,” *Geophys Res Lett*, vol. 48, no. 10, May 2021, doi: 10.1029/2020GL092326.

[77] NOAA, “Meteorological Observations.” Accessed: Nov. 08, 2023. [Online]. Available: https://tidesandcurrents.noaa.gov/stations.html?type=Meteorological+Observations

[78] Andres Tovar, “Inverse distance weight function,” MATLAB Central File Exchange. Accessed: Nov. 08, 2023. [Online]. Available: https://www.mathworks.com/matlabcentral/fileexchange/46350-inverse-distance-weight-function